Spring 2-10-2020

Inhibiting Surface Flashover in Vacuum with High Gradient Insulators

Cameron Harjes
University of New Mexico

Cameron Harjes

Candidate

Electrical and Computer Engineering

Department

This thesis is approved, and it is acceptable in quality and form for publication:

Approved by the Thesis Committee:

Jane Lehr, Chairperson

Mark Gilmore

Lisa Fisher

Andrew Fierro

INHIBITING SURFACE FLASHOVER IN VACUUM WITH HIGH GRADIENT INSULATORS

By

CAMERON HARJES

B.S., ELECTRICAL ENGINEERING, UNIVERSITY OF NEW MEXICO, 2017

THESIS

Submitted in Partial Fulfillment of the
Requirements for the Degree of

Master of Science
Electrical Engineering

The University of New Mexico
Albuquerque, New Mexico

May 2020

Acknowledgements

I am very grateful to my parents Chuck and Sandi Harjes, who have supported me throughout my life and academic career. I am also grateful for my loving girlfriend and my other family members who have encouraged me along the way. I would also like to thank my advisor Dr. Jane Lehr and the other members of the Aperiodic lab group.

This work was sponsored by the Office of Naval Research (ONR), under grant number N00014 - 17-1-2848. The views and conclusions contained herein are those of the authors only and should not be interpreted as representing those of ONR, the U.S. Navy or the U.S. Government.

Inhibiting Surface Flashover in Vacuum with High Gradient Insulators

By

Cameron Harjes

B.S., Electrical Engineering, University of New Mexico, 2017

M.S., Electrical Engineering, University of New Mexico, 2019

Abstract

In high voltage systems, insulators may be used to separate conductors and these insulators are typically the limiting factor in the system's operating voltage. When the voltage between two conductors is too large, the insulators can fail due to surface flashover. As systems become more compact, the threat of failure by insulator flashover increases, making the optimization of insulators a critical task for reliability.

Insulators at a vacuum interface are especially vulnerable to surface flashover. Insulators have been shown to holdoff more voltage in vacuum after being baked to remove imbedded surface gases. Ceramic materials are particularly attractive because, unlike polymers, they can be baked at very high temperatures without damage. To further increase the holdoff voltage, ceramic was configured as a high gradient insulator. A high gradient insulator is a stack of alternating layers of insulating and conducting material which has been shown to increase the holdoff voltage, under certain conditions. In this work, two approaches to high gradient insulators are explored.

Table of Contents

List of Figures

List of Tables

Chapter 1

Introduction

1.1 Background

In pulsed power systems it is necessary to use insulating materials to separate conductors having different potentials. These insulators can be made from many different materials and can have varying geometries. This variability is utilized to increase how much electric field the insulator can tolerate before succumbing to surface flashover or breakdown through the bulk. This threshold is called the holdoff voltage of the insulator. Pulsed power systems commonly fail due to vacuum surface flashover along the surface of the insulator. Improving insulator technology will lead to higher voltage capability and more reliability in experimentation. To investigate what modifications can increase the holdoff voltage, it is beneficial to understand how vacuum surface flashover occurs. Secondary electron emission avalanche (SEEA) is a dominant theory of how vacuum surface flashover forms [1]. SEEA is the theory that electrons emitted at the cathode triple point are accelerated by the potential and collide with the surface of the insulator. The energy from the impact releases gas molecules and more electrons from the insulator's surface, potentially leaving a net charge on this region of the insulator [2]. These freed electrons are then accelerated by the potential until they also collide with the surface of the insulator releasing even more electrons. These electrons can also collide with gasses released from the surface, potentially resulting in ionization. These effects accumulate until a current path, via the electrons along the surface and ionized gas molecules, is formed. Minimizing the avalanche could improve the maximum holdoff voltage achieved by the insulator.

The experimental results show how changing the geometry and material of an insulator effects the holdoff voltage. Insulators were placed in a vacuum chamber and stressed using

increasing levels of pulsed voltage until vacuum surface flashover occurred. The breakdown voltage was recorded and the holdoff electric field was calculated. Using a current viewing resistor and a D-dot the voltage and current supplied by the Marx bank were monitored. Changes in the voltage and current waveforms clearly indicated that vacuum surface flashover had occurred.

1.2 Motivation

High voltage experiments often have vacuum sections separated from oil filled sections. The material used to separate these sections needs to be a vacuum compatible insulator. Aluminum Nitrate (AlN) is a vacuum compatible ceramic insulator that can be baked at 400°C. This material is optimal for high voltage experiments that require vacuum compatible insulators, however data needs to be collected on the holdoff voltage of the material. Previous experiments have successfully increased the holdoff voltage by modifying the insulator or shaping the electric field [1] [3]. This thesis discusses similar experiments done on the AlN insulator to compare results.

In pursuit of a larger holdoff voltage, the AlN insulator was modified to be a high gradient insulator. A high gradient insulator (HGI) is an insulator composed of alternating conducting and insulating layers. Although HGIs have been shown to increase the holdoff voltage [4], much remains unknown about the optimal geometry because HGI analysis often resists generalization with results limited to specific geometries [5].The University of New Mexico Aperiodic lab in association with Sienna technologies have tested different styles of HGIs in order to confirm what has been reported in the literature and test what design factors are crucial for HGI maximum holdoff voltage. Figure 1.1 is a HGI made from alternating layers of insulating ALN and conducting molybdenum.

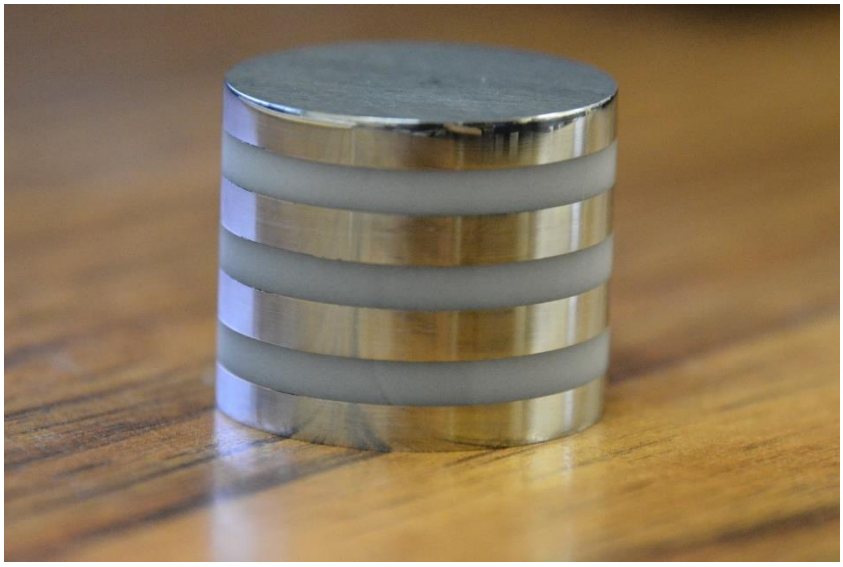

Figure 1-1: A high gradient insulator made of alternating thick layers of AlN and Mo constructed by Sienna Technologies.

To date the dominant styles for optimal HGI design focus on the insulator to metal (I/M) ratio. Leopold et al suggested that optimal design approaches an I/M ratio approaching 3 using a few thick layers of material. Leopold argued that if the conducting layers were not significantly thick the electric field modifications would not be strong enough to push electrons away from the surface of the insulator [6]. Figure 1.1 shows a Leopold style high gradient insulator with an I/M ratio of 1. Livermore et al have results that show an I/M ratio that approaches infinity is the optimal design for HGIs [7]. However, the Livermore group used insulators having many thin layers of conducting and insulating material as seen in figure 1.2. Their results are consistent with the idea that an HGI is a group of stacked small insulators separated by a conductor, making use of the observation that the electric field holdoff increases as the length of the sample decreases [8]. Another difference in the designs is the first layer material. The Leopold group used a conducting layer first to press against the cathode and therefore shaped the electric field at the triple point, however the Livermore group used an insulating layer first. Both groups tested

large and small numbers of I/M ratio, but their results do not align with each other. UNM in association with Sienna technologies made both Leopold and Livermore style HGIs and compared the results to try and reconcile the conflicts in the literature. This work will show that both styles of HGIs are effective, but the many thin layers appears to have a higher electric field holdoff value.

Figure 1-2: A high gradient insulator made of alternating layers thin of AlN and Cu.

Both styles of HGIs were able to improve the holdoff voltage value compared to the commonly used monolithic alumina insulators. This data was collected by placing these HGI's into a vacuum chamber and stressing them under high voltage until vacuum surface flashover occurred, as seen in figure 1.3.

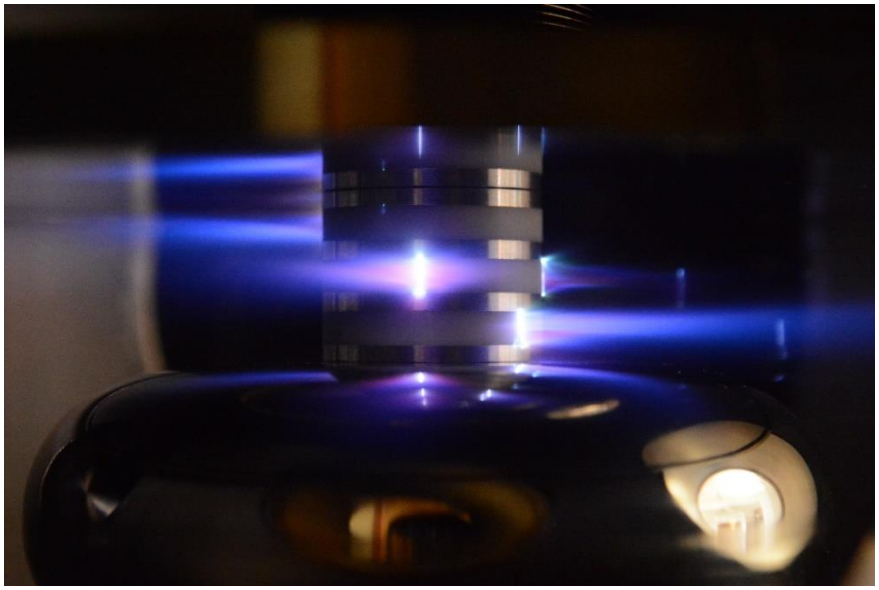

Figure 1-3: An HGI sample experiencing vacuum surface flashover. The anode is the bottom electrode and the cathode top electrode.

Chapter 2

Review of Related Literature

2.1 Triple point

High voltage systems often have points where insulators intersect with vacuum and metal. This point is referred to as the triple point. Vacuum surface flashover is believed to be initiated by electrons emitted at the cathode triple point, the point where the cathode conductor intersects with the insulator and vacuum as seen in figure 2.1. Figure 2.1 shows the triple point and the associated equipotential lines [1]. As the electrode potential is increased, electrons emitted from the cathode will be accelerated by the potential and drift in the direction of the electric field lines. These emitted electrons can bombard the surface of the insulator releasing electrons from the surface of the insulator eventually leading to vacuum surface flashover.

Shaping the electric field near the triple point is done to increase the amount of voltage the insulator can holdoff before succumbing to vacuum surface flashover [1] [3].

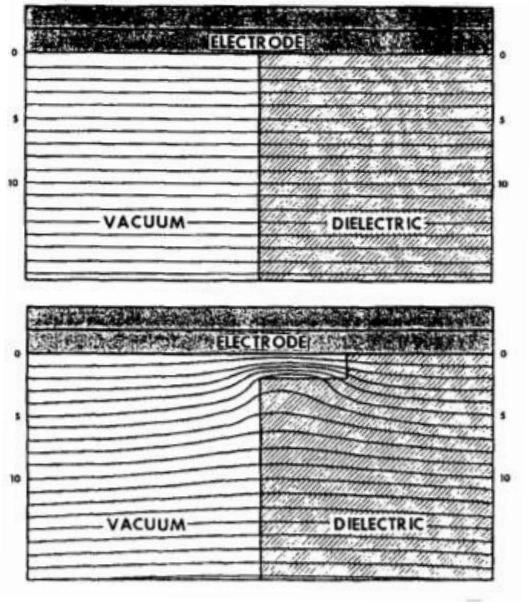

Figure 2-1: Equipotential lines next to the triple point [1]. Top figure shows an ideal junction. Bottom figure shows the effect of a void at the junction which increases the field strength and can bend an electron's trajectory towards the dielectric surface.

Conical insulators have been shown to increase holdoff voltage compared to cylindrical insulators [8]. Depending on orientation of the cone, simulations show that the electric field lines either encourage electrons to move away from the surface of the insulator or toward the surface [3]. This has been confirmed experimentally, by showing conical insulators holdoff more voltage when the large diameter intersects the cathode as seen in figure 2.2 [8]. This orientation is also known called a positive angle cone.

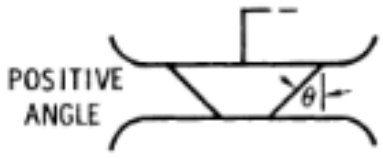

Figure 2-2: Positive angle conical insulator. Larger diameter against cathode [8].

Positive angle cones force electrons emitted from the cathode away from the surface of the insulator and negative angle cones force electrons to bombard the surface of the insulator [3]. By utilizing the natural electric field across the gap the holdoff voltage has been increased, however changes in geometry are not always practical.

Field shaping, manipulation of the electric field, can be accomplished by modifying the electrode/insulator interface. Having a recess in the electrodes as well as having electrodes plug into the insulator have both shown to increase the holdoff voltage [9]. However, modifications at the cathode triple point have a larger effect [10]. These modifications, also known as cathode and anode shielding, change the electric field lines at the triple point and force electrons away from the insulator's surface increasing the holdoff voltage. Figure 2.3 is an example of cathode and anode shielding.

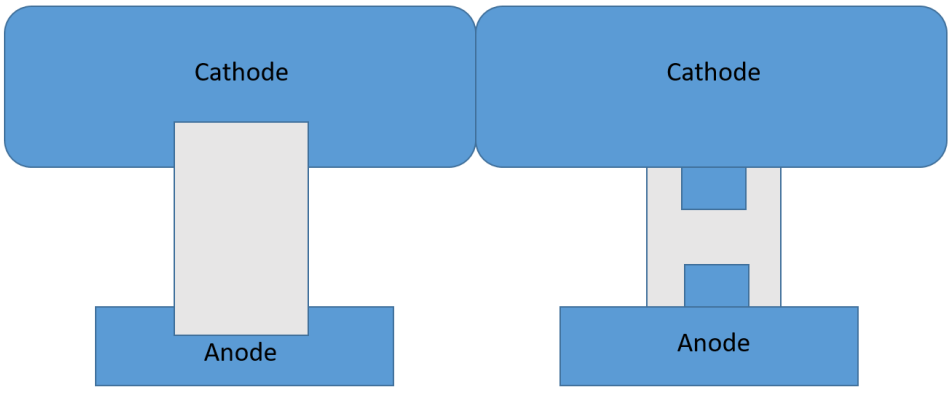

Figure 2-3: Anode and Cathode shielding. Metal inserts inside the insulator and recessed electrodes.

2.2 Secondary Electron Emission yield

The amount of energy required for an electron to be emitted from a material depends on the materials work function [11]. High electric fields are present at the cathode triple point and because of this electrons can overcome the work function and emit, which is called field emission. The freed electron is accelerated by the potential and bombards the insulator. The number of electrons emitted will depend non-linearly on the energy of impact and the materials work function. This is because as the incident energy is initially increased above the work function, more electrons are freed from the impact but as the incident energy gets even larger the electron can bury itself deep into the insulator material releasing fewer electrons. The deeper inside the material the electron buries itself the less probable it can escape, let alone emit additional electrons to feed an avalanche [12]. Each insulator material has a unique curve to specify the number of electrons emitted depending on the incident electron's energy, called the yield curve. When designing high voltage experiments the materials chosen need to have a low yield.

Surface modification, like creating ridges, has been shown to impede the development of an electron avalanche [13]. Intentionally grooving the surface of a material will force emitted electrons into the grooves of the insulator as seen in figure 2.4. Electrons being forced deep into the groove walls helps suppress the amount of secondary electron yield generated by a material.

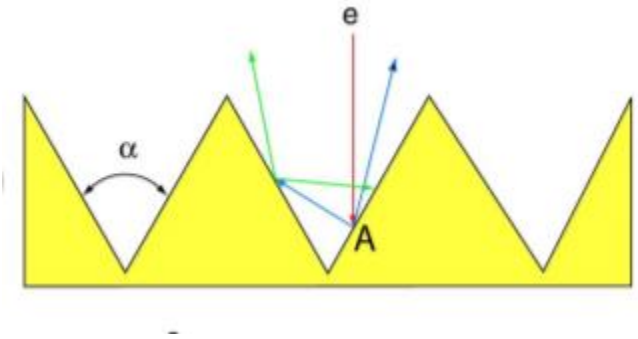

Figure 2-4: A grooved insulator surface forcing electrons to plummet into the insulator surface [13].

2.3 Outgassing

Outgassing is desorption of a materials surface gasses. Materials in high vacuum naturally desorb gas from the surface. For insulators, this process is accelerated by electron bombardment as seen in figure 2.5. Electrons that bombard the insulator not only free electrons, but also free gas molecules from the insulators surface. The gas molecules can be ionized by the electrons and contribute to the arc channel that makes up vacuum surface flashover plasma. The pressure of the gas along the surface during a flashover event has been calculated to be 200 Pa [14]. This is equivalent to 1.5 torr and standard pressures for vacuum surface flashover experiments range from 10^{-5} to 10^{-7} torr. Spectroscopy data has been taken from the light generated by the plasma and CO, CO_2 and $H_2$are commonly found [14] [15]. This is thought to be from the insulators exposure to air.

Surface treatment, like glow discharge, baking and conditioning, have been shown to increase the holdoff voltage of the insulator [1] [16]. These treatments reduce the amount of gas present on the insulators surface. More energetic electron bombardments are required to free the gas molecules deeper in the surface of the insulator. Because more energetic electrons are required the total voltage must increase and therefore the holdoff voltage is increased.

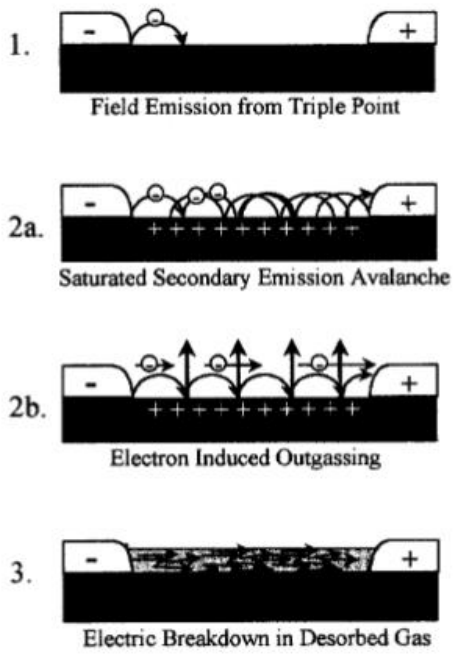

Figure 2-5: A representation of how field emission leads to outgassing then electric breakdown [15].

2.4 Secondary Electron Emission Avalanche

Secondary Electron Emission Avalanche (SEEA) is the dominant theory of how vacuum surface flashover occurs. SEEA is the theory that electrons emitted at the cathode triple point are accelerated by the potential and bombard the surface of the insulator [2]. The energy from the impact overcomes the materials work function and releases secondary electrons. The secondary electrons are accelerated by the potential until they also bombard the surface of the insulator releasing even more electrons. Electron induced outgassing occurs and as the neutral gas molecules drift they are impacted by electrons and ionized. As the insulator loses electrons a positive surface charge accumulates near the cathode triple point [2]. This enhances the electric field causing more electrons to bombard the surface releasing even more electrons and gas molecules. This effect accumulates until an avalanche of electrons is present on the surface and

ionized gas is present above the surface. These two mechanisms assist in breakdown and a current path is formed. Figure 2.6 is an illustration of the process of SEEA [14].

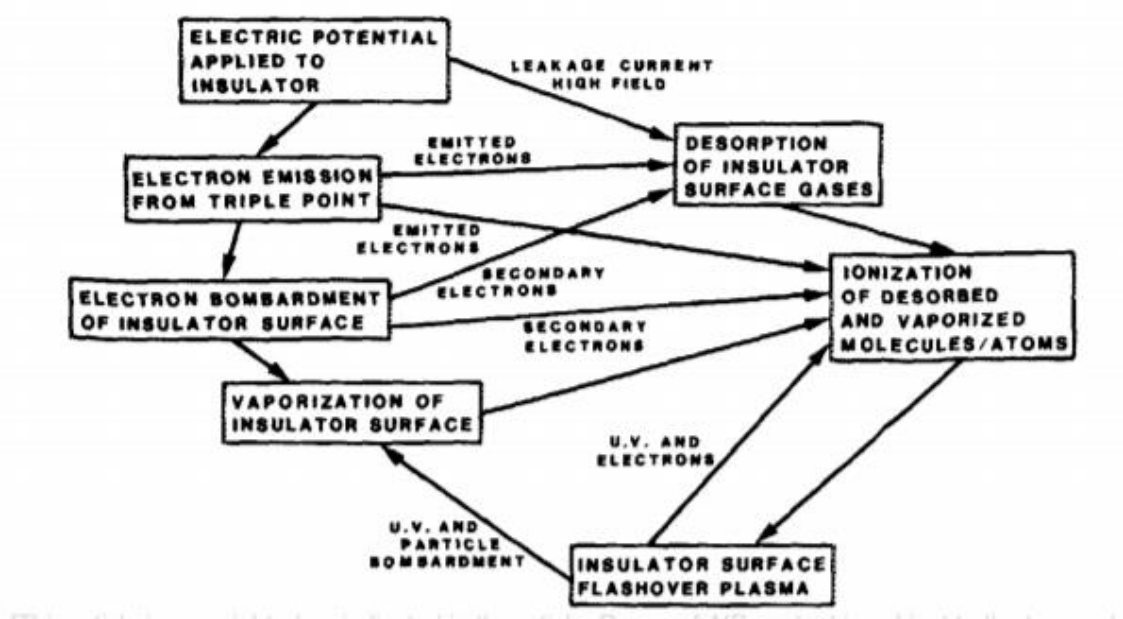

Figure 2-6: Illustration of the process of secondary electron emission avalanche culminating in surface flashover [14].

2.5 High Gradient Insulators

High Gradient Insulators (HGI), as seen in figure 1.1 and 1.2, are insulators composed of alternating layers of conducting and insulating materials. HGIs were first proposed by E. Gray in the 1980's [4]. Gray proposed that there is an increase in holdoff electric field because of the decrease in the length of the insulator. Stacking insulators became a way to increase the holdoff voltage while also taking advantage of higher electric field holdoff for smaller insulators. It has been reported that HGIs are able to holdoff 1.5 to 4 times the electric field compared to a monolithic insulator of the same style [4].

The significant improvement demonstrated by HGIs attracted other researchers to continue experimentation. Researches began to experiment with the layers of the HGIs trying to optimize the design. It was believed that conducting layers were able to catch secondary electrons and therefore reduce the effect of SEEA. This led to experimenting with conducting layers having a larger diameter then the insulating layers. These tests showed that having HGI's with protruding conducting layers did not increase the holdoff voltage [4]. However, other experimenters began to evaluate the importance of the thickness of the conducting layer. Leopold et al (2005) showed that the electric field next to the surface of an insulator is changed by the conducting layer [6]. The electric field normal to the HGI pushes electrons away from the surface as seen in figure 2.8. However, he argued that if the conducting layer is not sufficiently thick compared to the insulating layer the electric field would not be strong enough to push incident electrons away. An optimal insulator to metal ratio (I/M) was proposed to be 3 because at this and higher ratios coupling can occur between cells. This means that electrons generated from collisions on one insulating layer are able to collide with the next layer, rather than being pushed away from the surface as seen in figure 2.8 [5]. However, this experimental result was obtained while varying I/M while maintaining an I+M cell length of 4mm. Thus, it is unclear if the I/M ratio of 3, or a metal layer minimum thickness of 1 mm, or an insulating layer with a maximum thickness of 3mm is the real limiting factor for cell coupling, and therefor optimization.

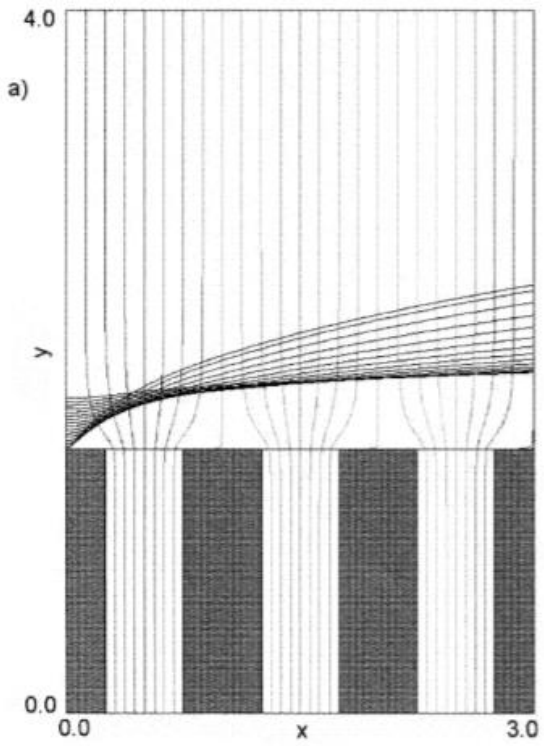

Figure 2-7: Simulation of the electric field next to the surface of an HGI [5].

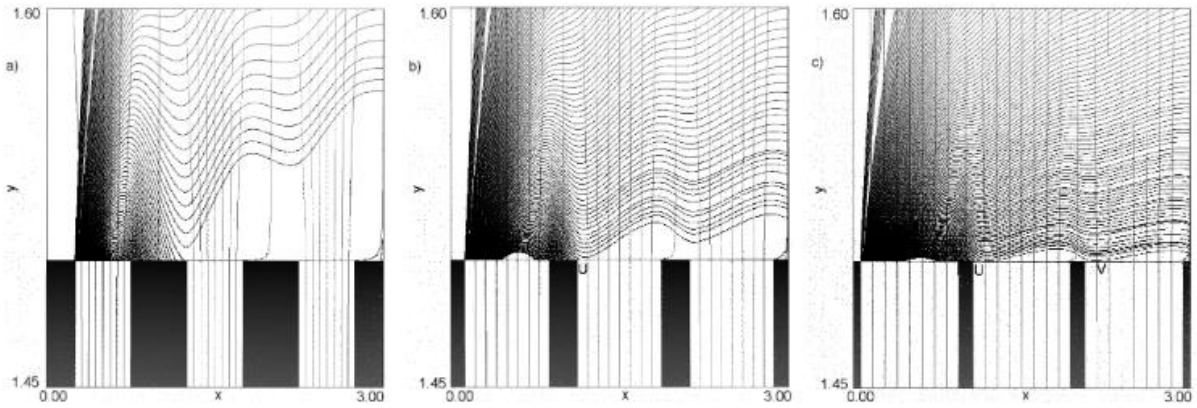

Figure 2-8: Simulation showing the electron trajectories from the cathode triple point. An I/M ratio of 1 (left) shows how the metal layers push electrons away from the adjacent insulating layer. An I/M ratio of 3 (middle) shows a similar result to an I/M ratio of 1, however electron trajectories are closer to the surface. An I/M ratio of 7 (right) shows how cell coupling can occur as the ratio gets to large [5].

In a different experiment conducted by Livermore the holdoff electric field increased with increasing I/M [7]. However, there are several differences between the experiments. The first layer was metal for the Leopold group and insulator for the Livermore group. Leopold used insulators having a few thick conducting layers and Livermore used insulators having many thin conducting layers. For Livermore, the total length of each sample ranges from 5mm to 12mm, the I/M ratio ranged from 20 to 100 for most samples (a few were tested at a ratio near 1), and the insulator layer length ranged from 0.26mm to 1.3mm. For Leopold, the total lengths were between 16mm to 20 mm, the I/M ratios were varied from 0.32 to 6 (one was tested approaching 20), the I+M length was held constant at 4. Because the total length of the sample was controlled, changes in the I/M ratio changed the layer length. Large I/M would lead to very thin conducting layers. Harris et al tried to resolve the discrepant results by proposing that for thin layered HGIs the dominate breakdown mechanism is vacuum arcing between conducting layers and for thick layered HGIs the dominate breakdown mechanism is vacuum surface flashover [17]. Sampayan and Gray proposed that an HGIs should be a stack of small insulators and that the driving benefit of this design is the increase of electric field holdoff as there is a decrease in insulator length [4]. According to this proposition as I/M approaches zero the electric field holdoff should increase, however both Leopold and Livermore showed that this was not the case.

Chapter 3

Methodology

3.1 Experimental Setup

The surface flashover apparatus consists of a vacuum chamber capable of 10^{-7}Torr and a pressurized Marx bank that can deliver a 500kV, 500ns pulse. The vacuum chamber and Marx bank are separated by an insulating vacuum feedthrough. The vacuum feedthrough separates

different pressures and the high voltage anode from the grounded walls of the chamber. An insulator is placed between the anode and cathode inside the vacuum chamber. When the desired pressure is reached, the insulator is stressed by a high voltage pulse and the systems response is monitored by a capacitive probe called a D-dot and T&M research products current viewing resistor [18]. These diagnostics are located at the output of the Marx and are fed through the walls of the vacuum feedthrough, this keeps the diagnostics out of the vacuum section as seen in Figure 3.1.

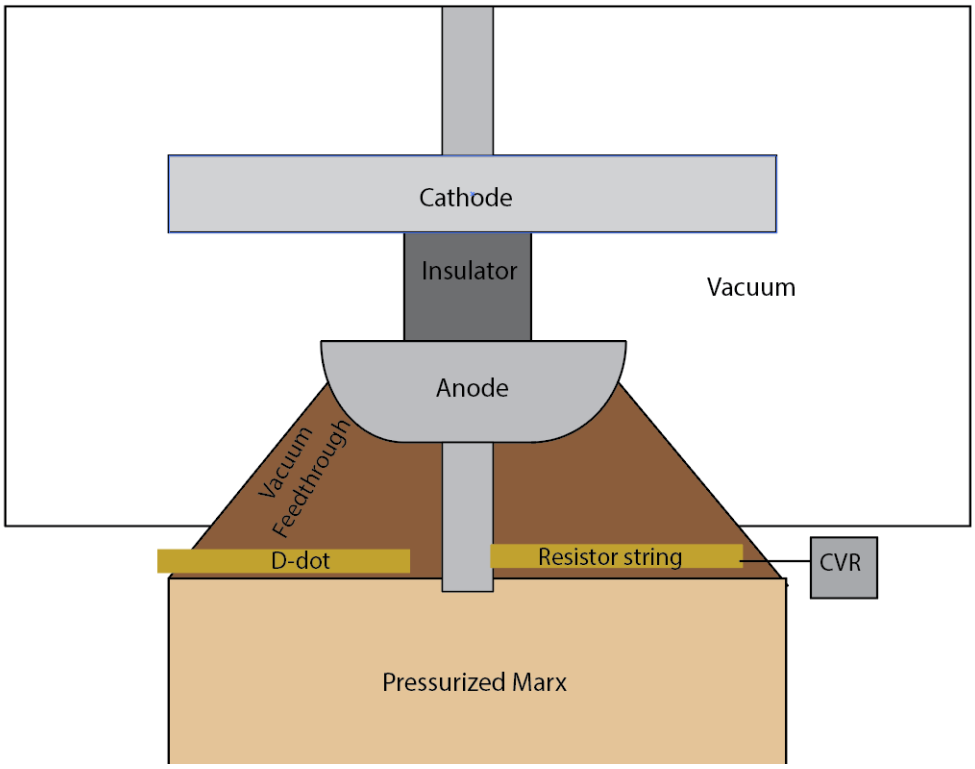

Figure 3-1: Illustration of the test insulators position during experimentation.

The integrated system, as seen if Figure 3.2, is mounted to a U-strut structure via rubber vibration mounts for stability and ground loop isolation. Control of the Marx is handled by a trigger circuit and vacuum is achieved by a scroll pump in line with a turbo pump.

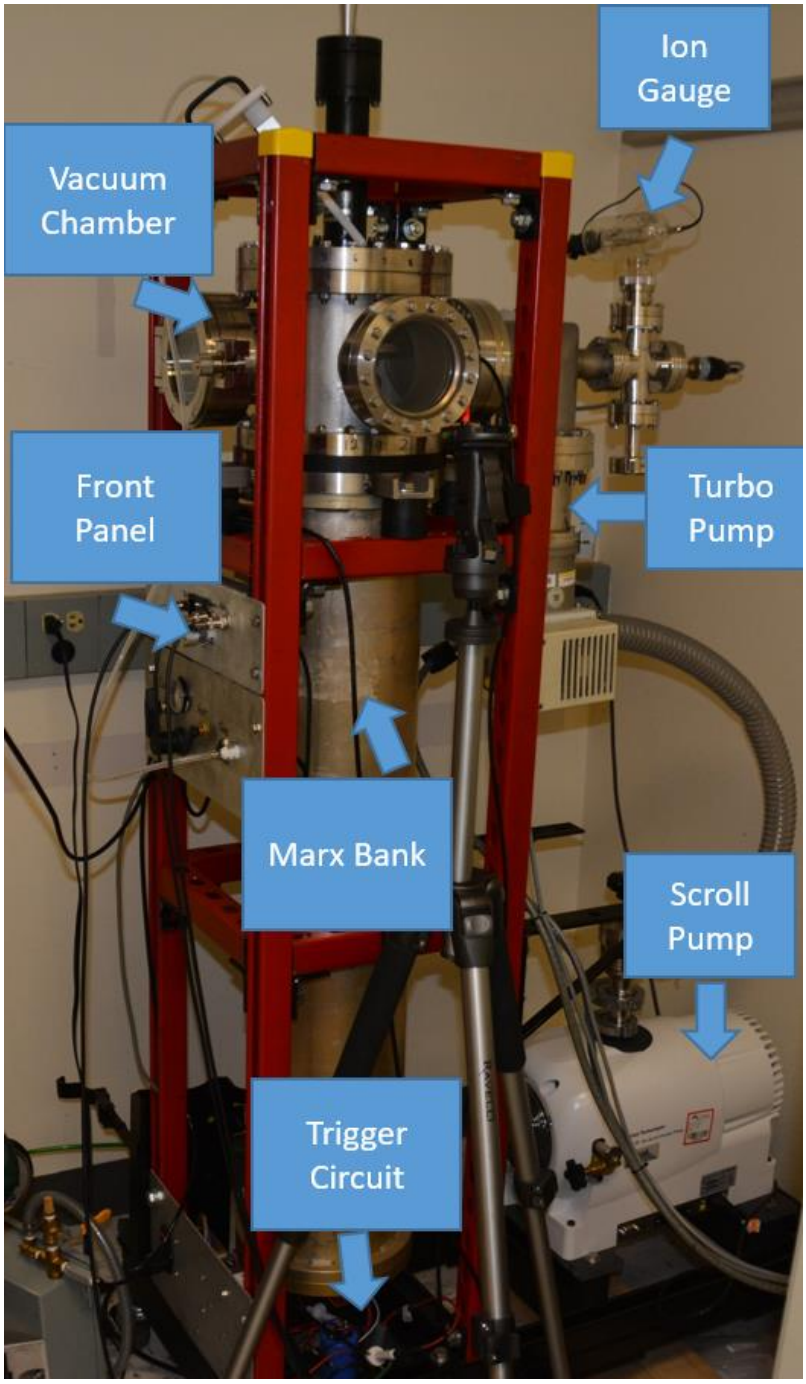

Figure 3-2: The integrated experimental setup

3.1.1 Vacuum Chamber

Figure 3.2 shows the vacuum chamber used for the experimental setup. The chamber is an 8-inch diameter stainless steel cylinder mounted to the Marx bank via the vacuum

feedthrough. The chamber has five available ports. A linear positioner is mounted to the top conflat as seen in Figure 3.3. The linear positioner controls the position of the cathode plate so insulators of varying lengths can be tested as seen in Figure 3.1. The chamber has three 6-inch side ports. These ports are used for insulator sample loading, a window for imaging diagnostics, and the turbo pump/ion gauge. Another side port is a 4.625-inch fitted with a blank conflat. Plans have been made to replace the blank conflate with a window/collimator for spectroscopy data.

3.1.2 Vacuum Pumps

A Pfeiffer Balzers turbo pump and controller are used to reduce the pressure to about 10^{-7}Torr. However, this turbo pump will not operate unless the starting pressure is about 0.1 Torr. An Allegiant technologies dry scroll vacuum pump is used in association with the turbo pump. The dry scroll pump reduces the pressure in the vacuum chamber to 10^{-2}Torr at which point the turbo pump can function. The pressure is monitored by an Allegiant technologies XGS 600 controller [19]. A thermocouple inside the controller is used to monitor the higher pressures ranging from atmospheric to 10^{-2}Torr and an ion gauge is used to measure the low pressures ranging from 10^{-4}Torr to 10^{-7}Torr. The dry scroll pump, turbo pump, and ion gauge are connected in line to one of the 6-inch ports on the vacuum chamber as seen in Figure 3.3.

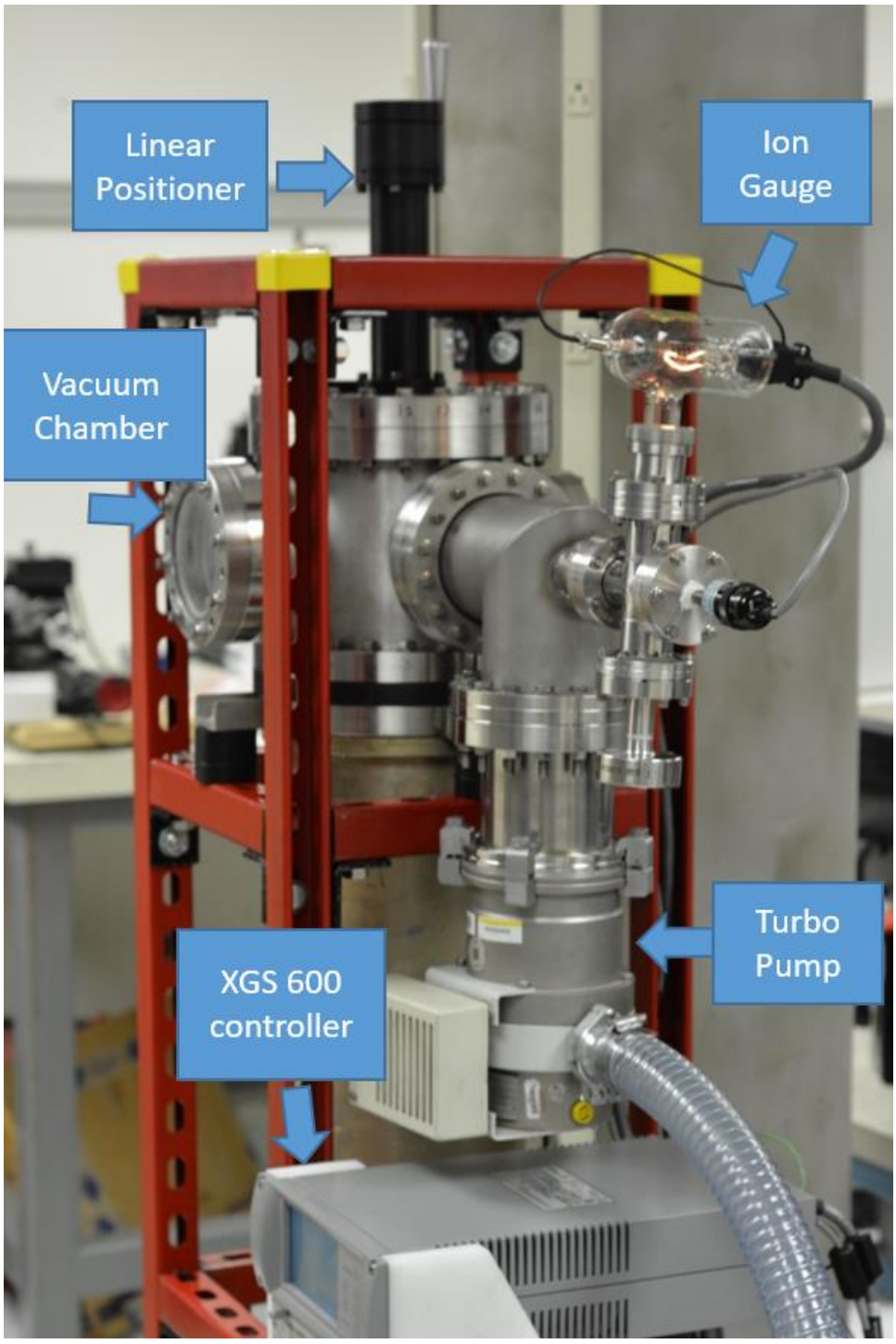

Figure 3-3: The turbo pump, ion gauge, and dry scroll pump connected to the vacuum chamber.

3.1.3 Marx Generator

A 500 ns high voltage pulse is generated by a 25 stage inverting Marx bank contained in an aluminum tube. The Marx is composed of Murata ceramic capacitors that are resistively charged through high voltage resistors as seen in Figure 3.4.

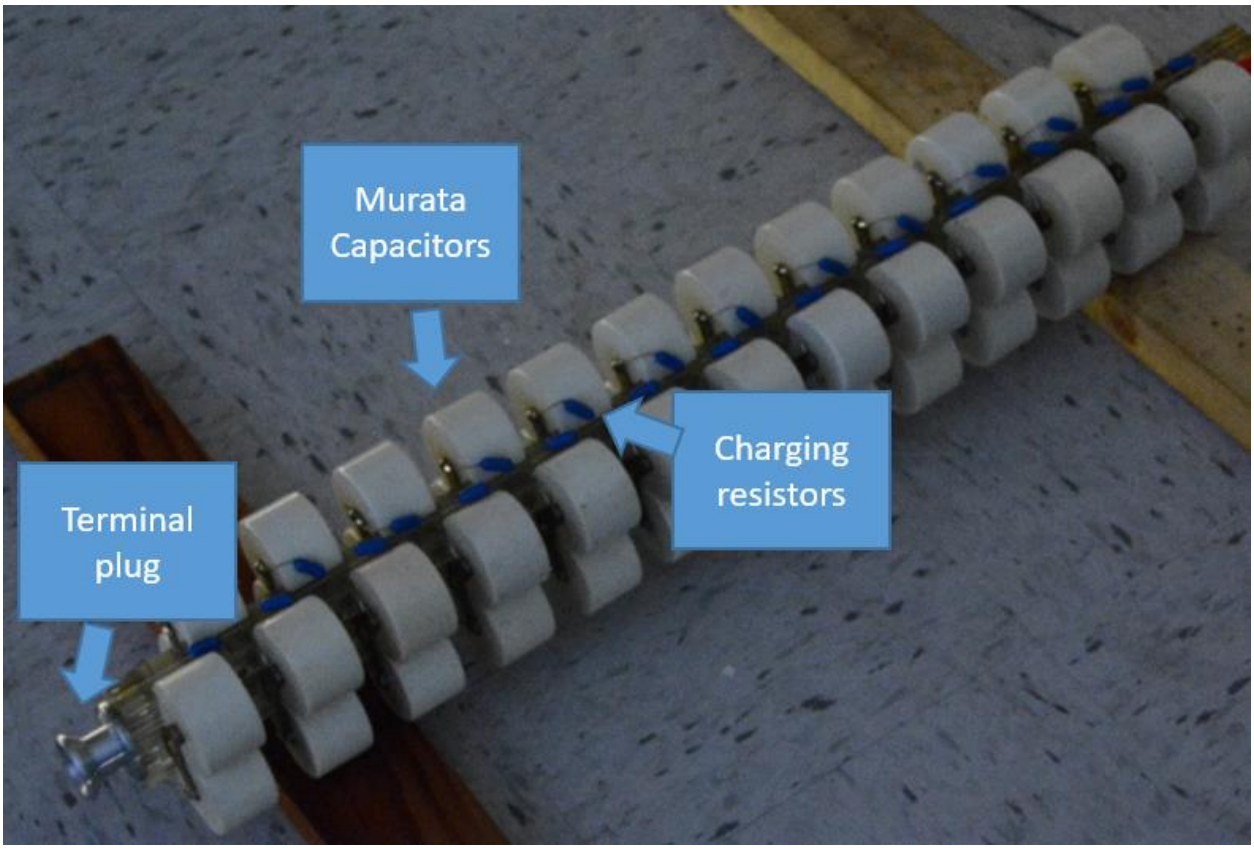

Figure 3-4: The Marx bank outside of the aluminum tube housing. The Murata capacitors are mounted to the insulating base. The terminal plug which attaches to the sodium carbonate solution resistor can be seen.

High voltage is provided by a negative polarity 35kV Gamma Research power supply. The Marx bank is designed to operate up to 1MV, however the operating voltage is limited to approximately 0.5MV due to vacuum surface flashover on the vacuum feedthrough. Charging of the capacitors can be varied by the user up to a maximum charge voltage of 35kV and as low as

4kV. The capacitors are mounted on an insulating base composed of two pieces that are screwed together using plastic screws as seen in figure 3.5. Between the insulating pieces are spark gaps that separate each stage. Each stage is composed of two 270nF capacitors and a 100Ω high voltage charging resistor connecting the adjacent group of capacitors. For user control, the first stage of the Marx bank is a trigatron style spark gap. The trigatron is operated by an ignition circuit used for motorized carts. Using a pulse generator the user sends a signal to the ignition circuit arcing the trigatron stage. If the other stages are charged to a voltage approaching self-break of the spark gaps, the Marx will erect with the trigatron stage supplying the high voltage pulse to the load. A plug connector is used to connect the output of the Marx to the anode. The Marx is terminated into a 460Ω sodium carbonate solution resistor in line with the anode as seen in Figure 3.5. The water resistor is in parallel with a 690Ω resistor string that is used in series with a current viewing resistor.

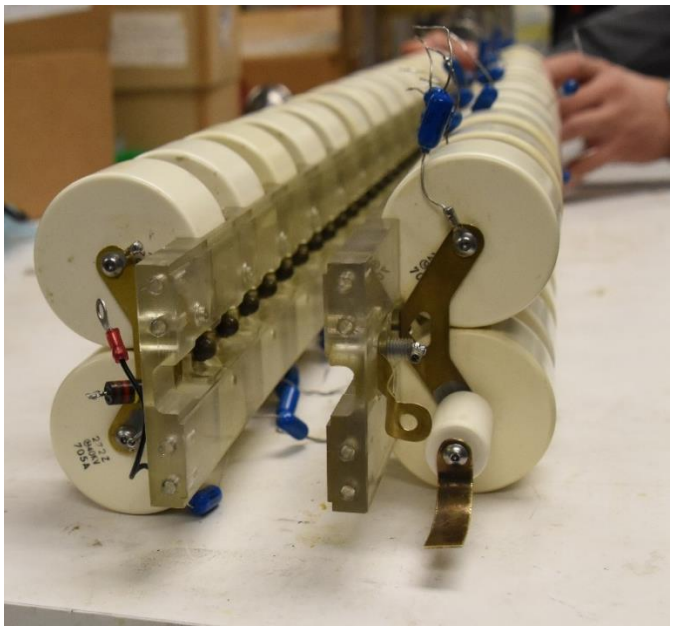

Figure 3-5: The Marx bank with the spark gaps showing.

The control panel, as seen in Figure 3.6, gives user control of the charge voltage and the pressure inside the Marx. In Albuquerque, New Mexico, atmospheric pressure is about 630 Torr. At this pressure the spark gaps inside the Marx will erect without a trigger pulse at a charge voltage around 9kV making the system uncontrolled. To operate at a larger charge voltage the Marx is filled with pressurized nitrogen. However, if the user wanted to use a charge voltage less than 9kV the Marx pressure is reduced below atmospheric pressure by an additional roughing pump. It is important for the Marx to operate at a voltage that is near self-break to ensure all of the stages erect. The pressure inside the Marx is varied with a regulator with serial communication ability. The user communicates with the controller via a custom LabVIEW program and sets a desired pressure [20]. The regulator has pressurized nitrogen and a roughing pump attached to its terminals. This allows for quick transitions between desired pressure settings.

Figure 3-6: This is the front panel of the experimental setup. This gives the user control of the pressurized nitrogen and the charge voltage.

The user can control the pressure and voltage settings from the control panel, or from an attached computer running a LabVIEW program. The front panel allows the user to direct nitrogen to the Marx or sample positioning tool seen in Figure 3.7. This tool was specially made to ensure that the insulator sample is placed on the anode at the same location every time. The tool consists of a pneumatic-powered gripper with long fingers mounted to a base that mates with the gate port of the vacuum chamber. The tool's fingers close when pressurized gas (nitrogen) is supplied to the actuator.

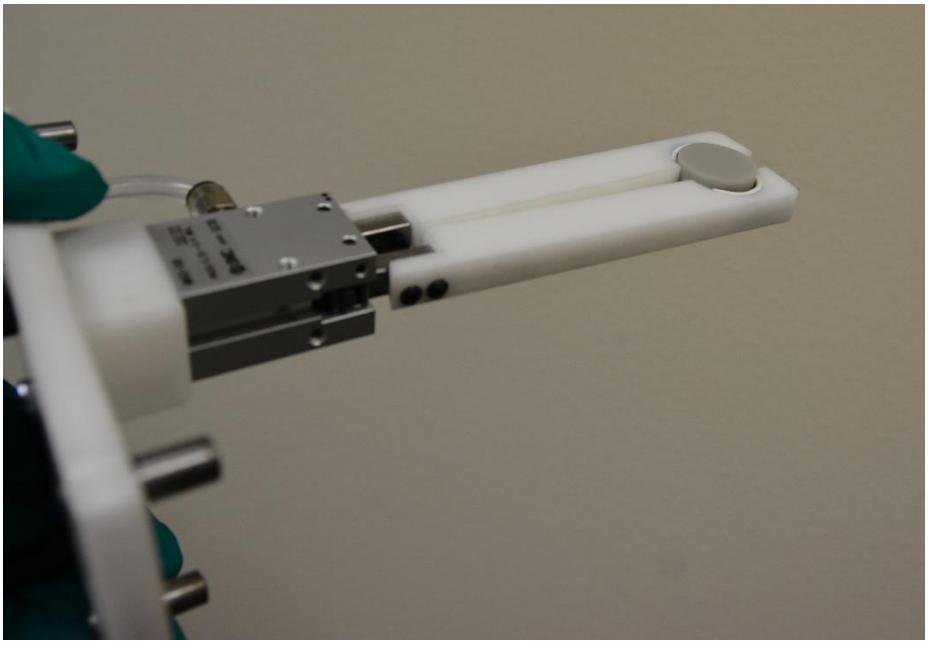

Figure 3-7: The sample positioning tool holding on to an insulator sample.

3.1.4 Vacuum Feedthrough

The vacuum feedthrough as seen in figure 3.8, is needed to separate sections of different pressures while allowing the voltage pulse to stress the insulator in vacuum. This is accomplished by allowing the anode to be fed through the Ultem (polyetherimide) vacuum feedthrough. Ultem has high dielectric and mechanical strength making it a good choice for the vacuum feedthrough [21]. The vacuum seal is maintained by two O-rings attached to the base of the anode. An adaptor is used to attach the vacuum chamber to the Marx bank through threaded holes on the vacuum feedthrough. This allows for a vacuum tight seal between the low and high pressure sections. The vacuum feedthrough attempts to separate the high voltage anode from the grounded walls of the vacuum chamber, however vacuum surface flashover can occur if there is enough voltage and the insulator sample is able to holdoff the voltage pulse.

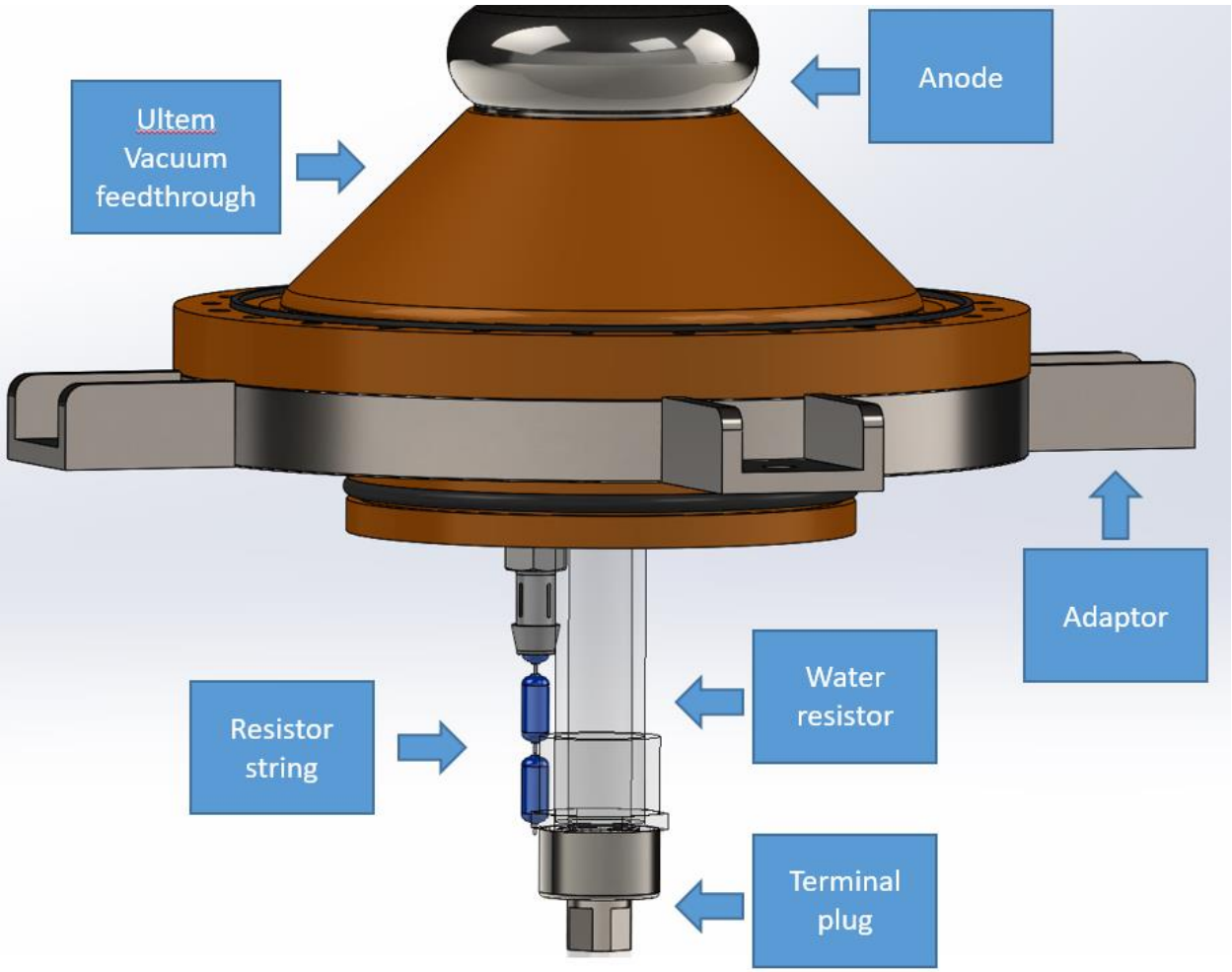

Figure 3-8: Model of the vacuum feedthrough.

When the Marx erects there is a potential between the anode and the walls of the vacuum chamber as shown in figure 3.9. In an ideal vacuum surface flashover experiment, the test insulator that is compressed between the anode and cathode will either experience vacuum surface flashover or holdoff the voltage pulse. However, in some cases the vacuum feedthrough insulator will fail due to vacuum surface flashover from the anode to the wall of the vacuum chamber. Figure 3.6 shows the CST simulations for the configuration [22]. Figure 3.10A shows the a test sample in the vacuum chamber, and Figure 3.10B shows the ultem insulator experiencing vacuum surface flashover between the anode and the vacuum chamber. The ultem

insulator was designed to have a conical shape in order to reduce the likelihood of vacuum surface flashover [8]. However, the CST simulations still show the possibility of flashover occurring along this surface. Ultem failure can be destructive and needs to be avoided.

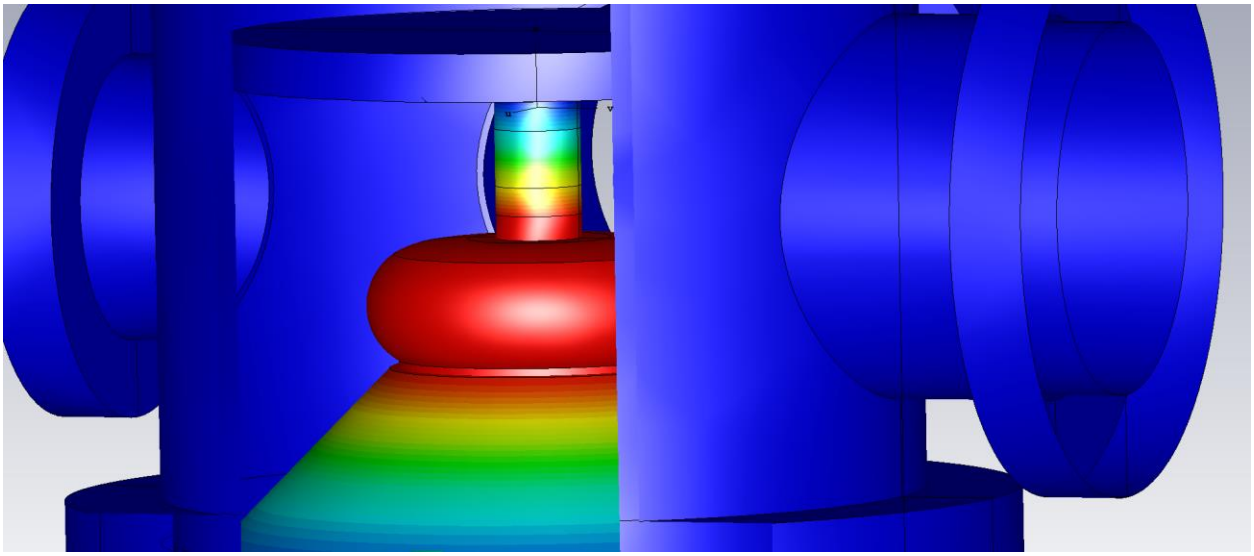

Figure 3-9: The above CST simulation shows the potential inside the vacuum chamber. It shows that it is possible for the ultem insulator to succumb to vacuum surface flashover. Red denotes high voltage and blue denotes ground.

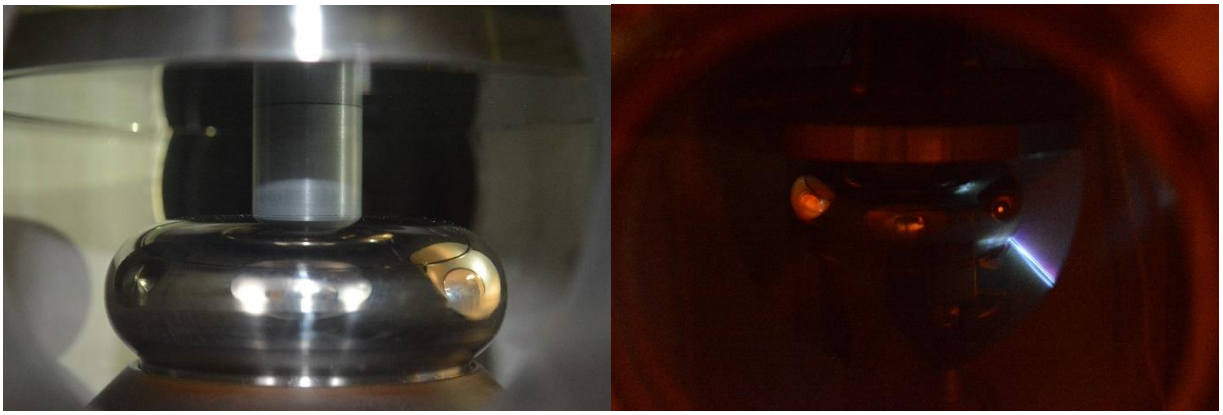

Figure 3-10: A test insulator in the vacuum chamber (A), the ultem insulator experiencing surface flashover (B).

3.1.5 Diagnostics

The experimental setup uses a D-dot and a current viewing resistor (CVR) as the diagnostic equipment. A D-dot is a capacitive probe that measures the voltage at the anode. Figure 3.11 shows the D-dot sensor mounted on the vacuum feedthrough. The D-dot sensor is made from a BNC cable with two strips of copper attached to the inner and outer conductors of the cable. The conducting strips increase the surface area of the conductors and therefore collects more signal from the voltage pulse generated by the Marx.

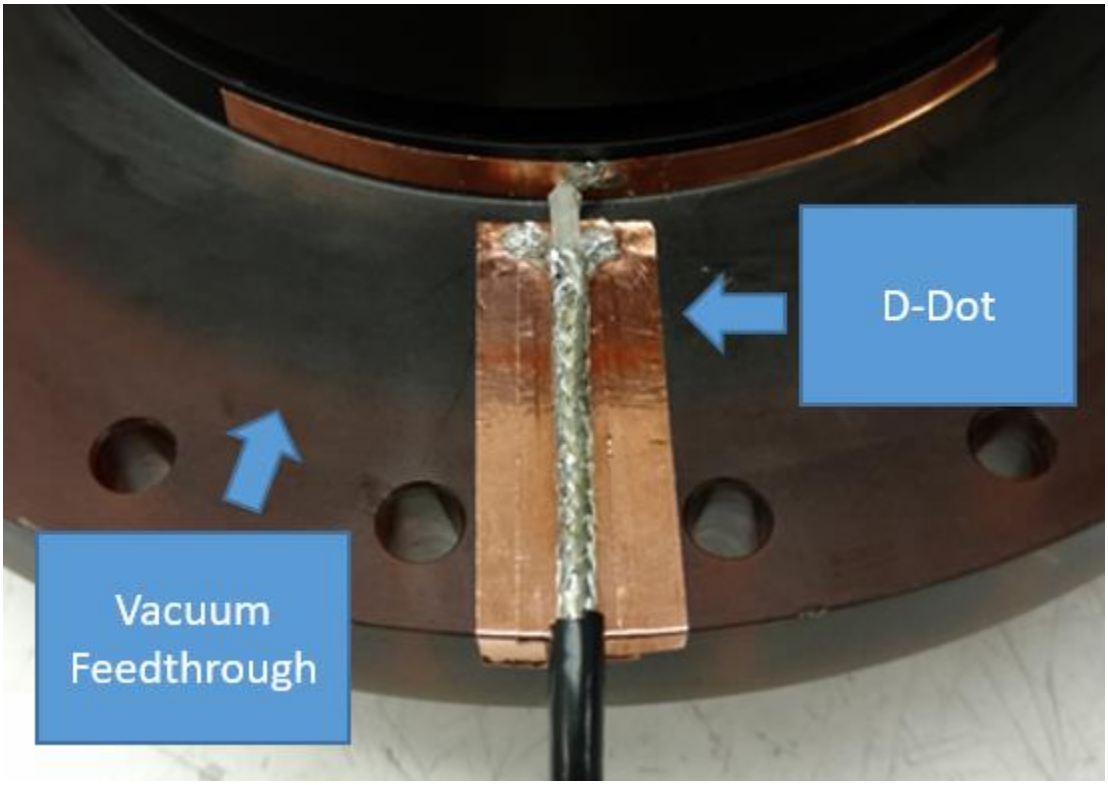

Figure 3-11 The D-dot sensor mounted on the ultem vacuum feedthrough. The center conducting copper strip has been reduced in size to improve the quality of the signal.

The D-dot was calibrated using a transmission line pulser and a Northstar PVM-4 high voltage probe as seen in Figure 3.12. The probe measures at 2000 to 1 and has a rise time of 2.5ns [23]. The transmission line pulser delivered a known voltage pulse into the load of the

Marx. The voltage probe and D-dot sensor made measurements in unison and the integrated D-dot signal was fitted to match the signal from the voltage probe. The D-dot sensor requires 40dB of attenuation due to the magnitude of signal collected.

Figure 3-12: The northstar probe with the transmission line pulse calibrating the D-dot sensor.

The other diagnostic used in this experimental setup is the T&M research products current viewing resistor. The CVR is connected to a string of high voltage resistors that are submerged in oil and connected to the load of the Marx as seen in Figure 3.13. Although the output of the Marx supplies more voltage than the resistors are rated for, early experimentation showed that if the resistors were submerged in oil flashover of the resistors did not occur. The current is measured through six high voltage resistors and the CVR connected in series for a total value of 680Ω.

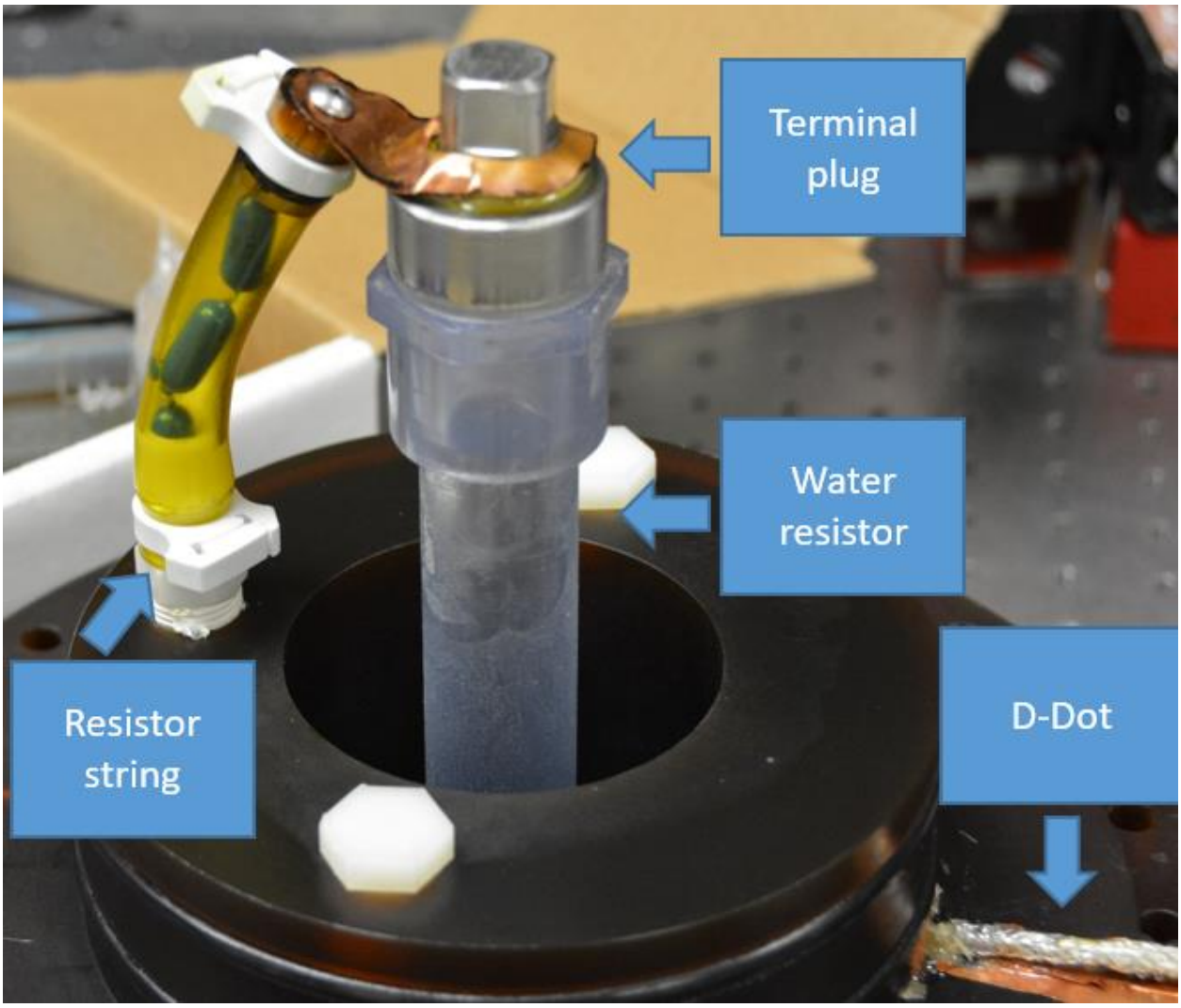

Figure 3-13: The current viewing resistor string attached to the water resistor. The water resistor and CVR string share a plug terminal with the output of the Marx.

The following waveforms show the expected results from the diagnostics when vacuum surface flashover does and does not occur. Because a D-dot sensor measures the electric field the signal needs to be integrated in order to analyze the corresponding voltage waveform. An example of the raw D-dot signal for a surface flashover event can be seen in Figure 3.14. As expected the voltage waveform of a surface flashover event rises quickly, but also falls quickly as seen in Figure 3.15. The raw D-dot signal for a holdoff event is noticeably different than a

surface flashover even as seen in Figure 3.16. The voltage waveform of a holdoff pulse rises quickly, but slowly dissipates to zero as seen in Figure 3.17. The current waveforms show a rise in current when the Marx erects and if no flashover occurs will dissipate to zero as seen in Figure 3.18. However, if a vacuum surface flashover event occurs the current waveform will rise with the erection of the Marx and then have another sharp fall and as seen in Figure 3.19. Using these diagnostics the voltage across the insulator is recorded and the waveforms confirm if a surface flashover event occurred.

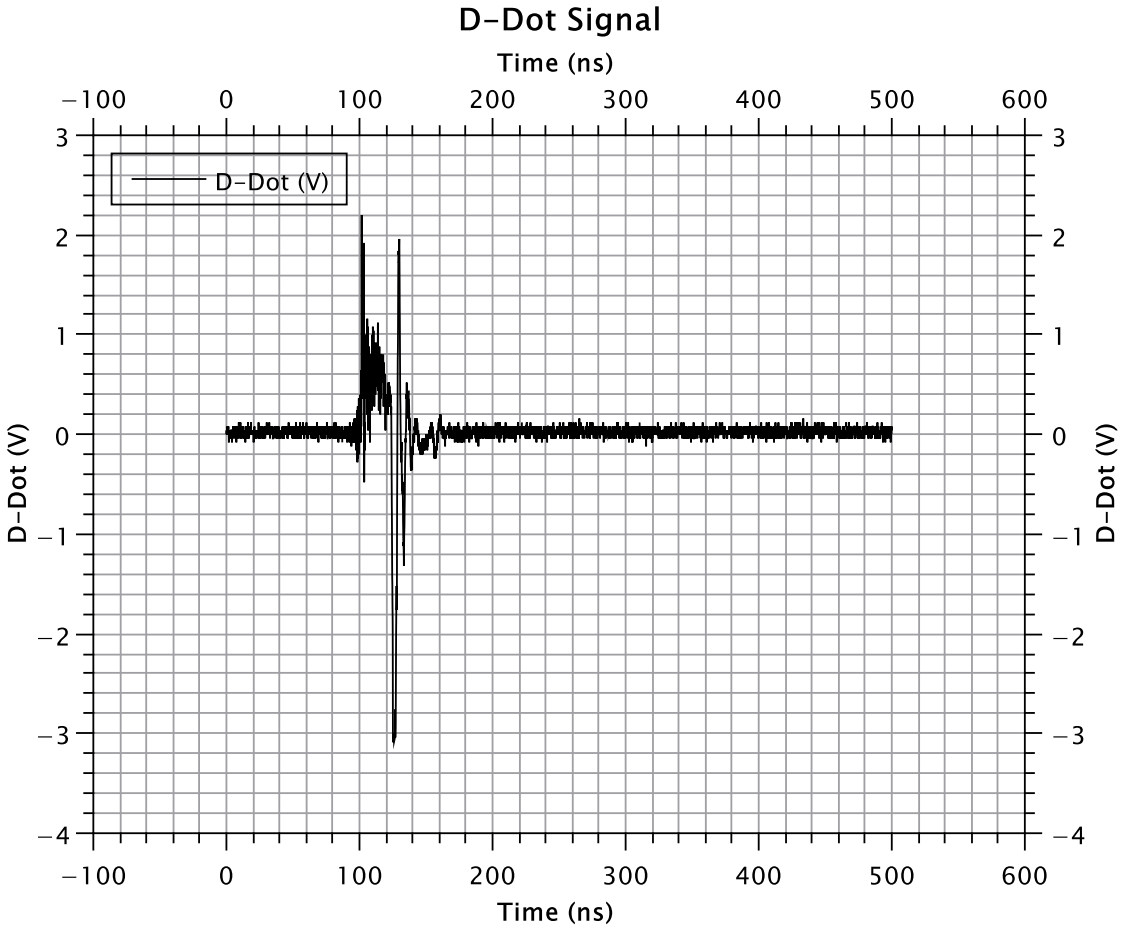

Figure 3-14: The raw D-dot signal for a surface flashover event.

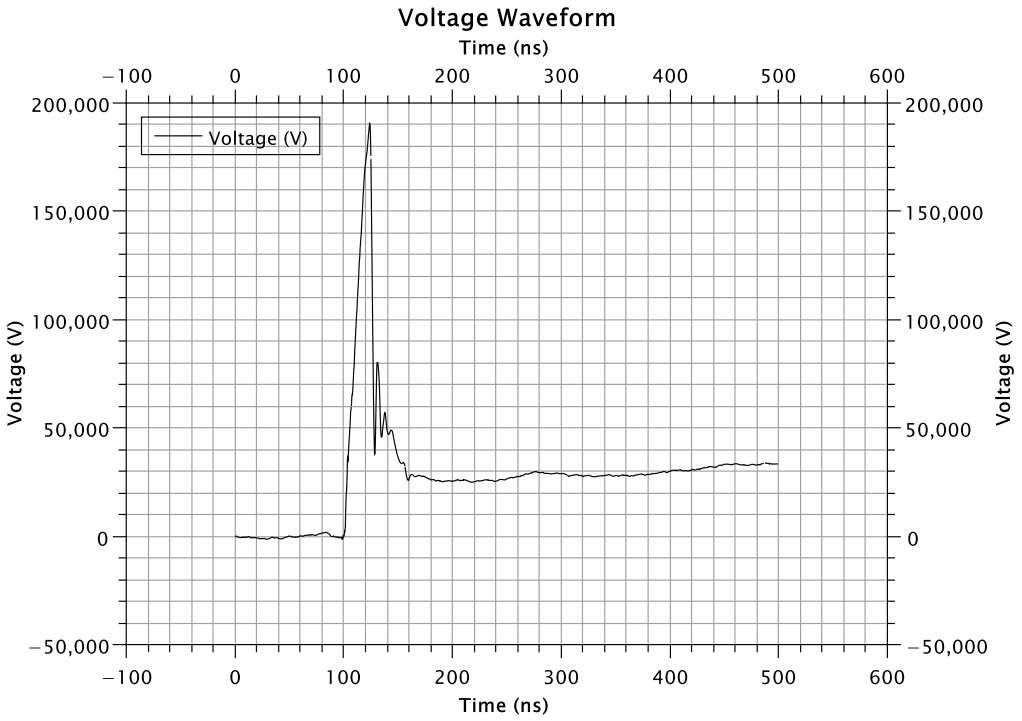

Figure 3-15: The voltage waveform for a surface flashover event.

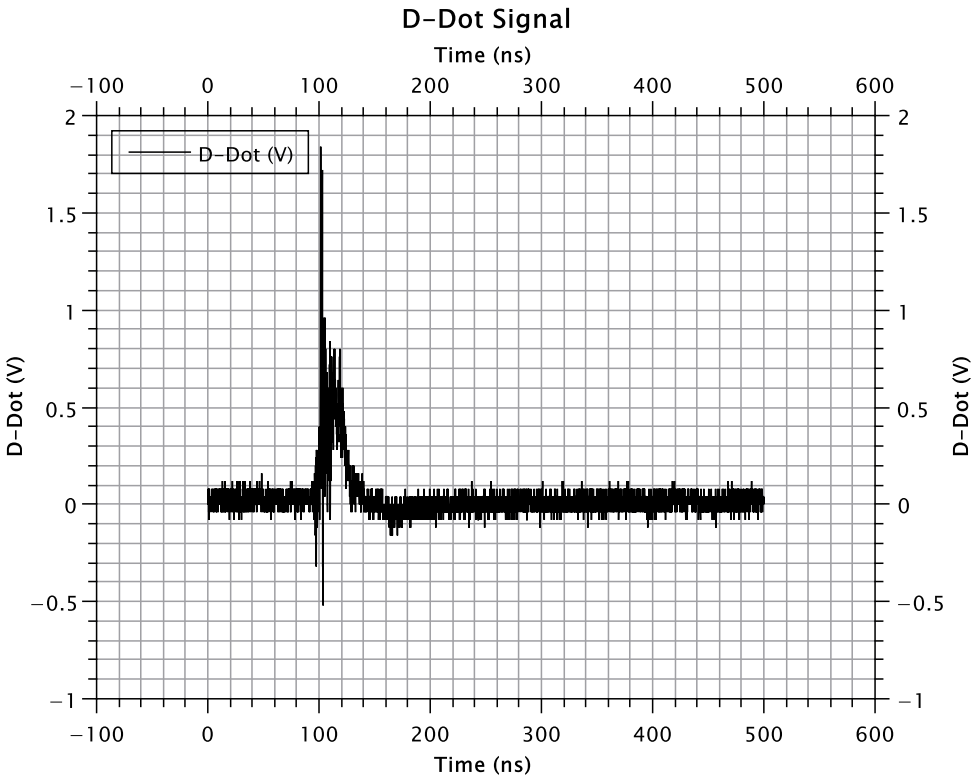

Figure 3-16: The raw D-dot signal for a holdoff event.

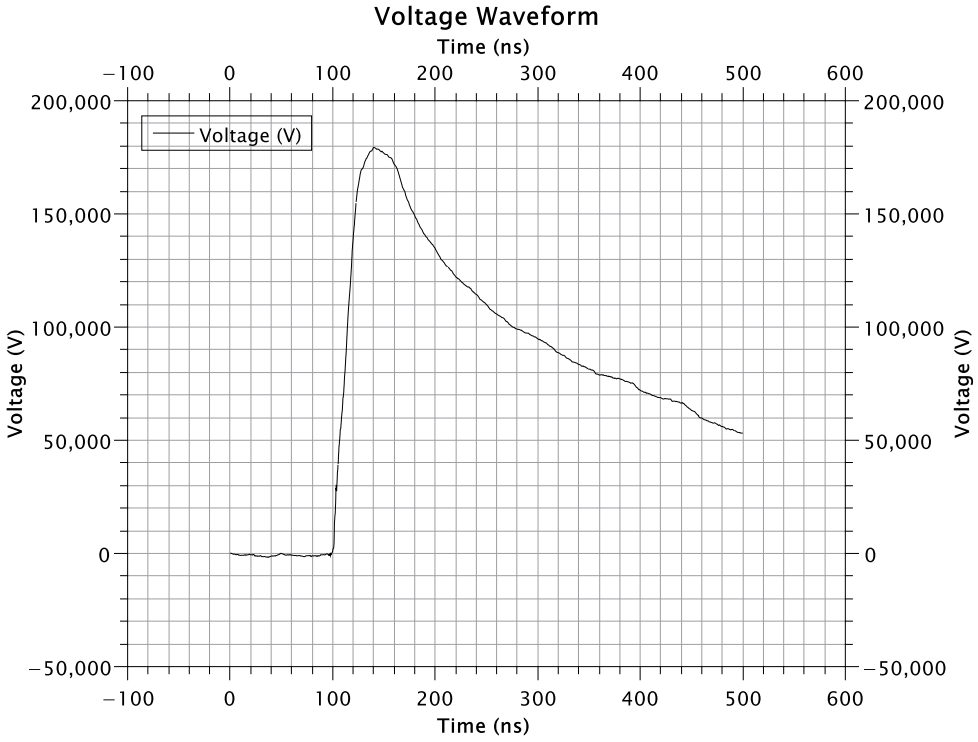

Figure 3-17: Voltage waveform of a holdoff event.

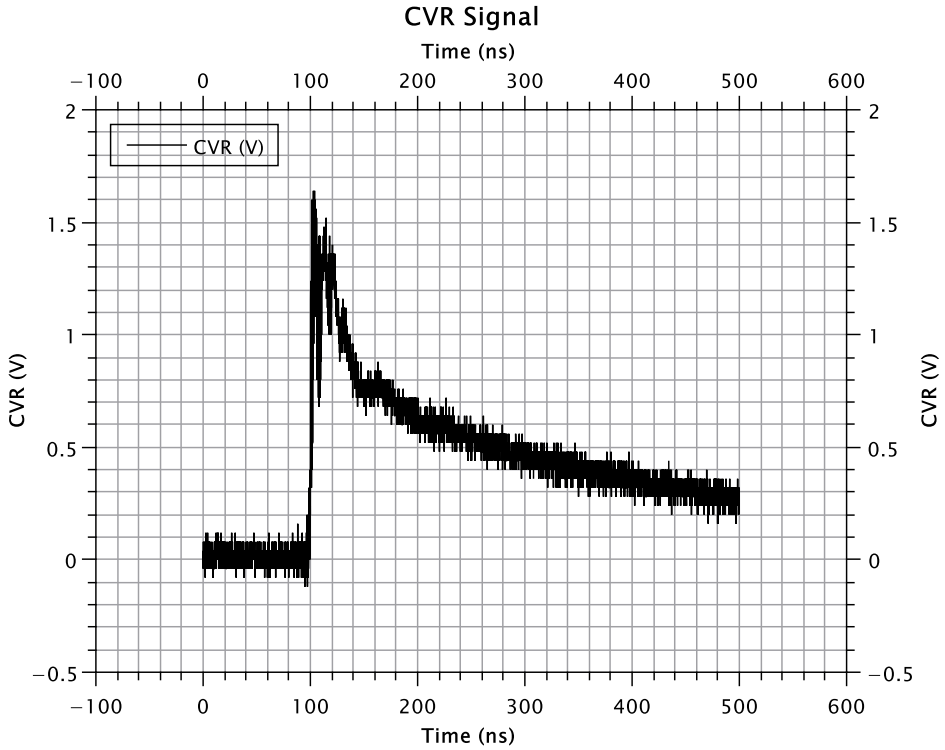

Figure 3-18: CVR signal from a holdoff event.

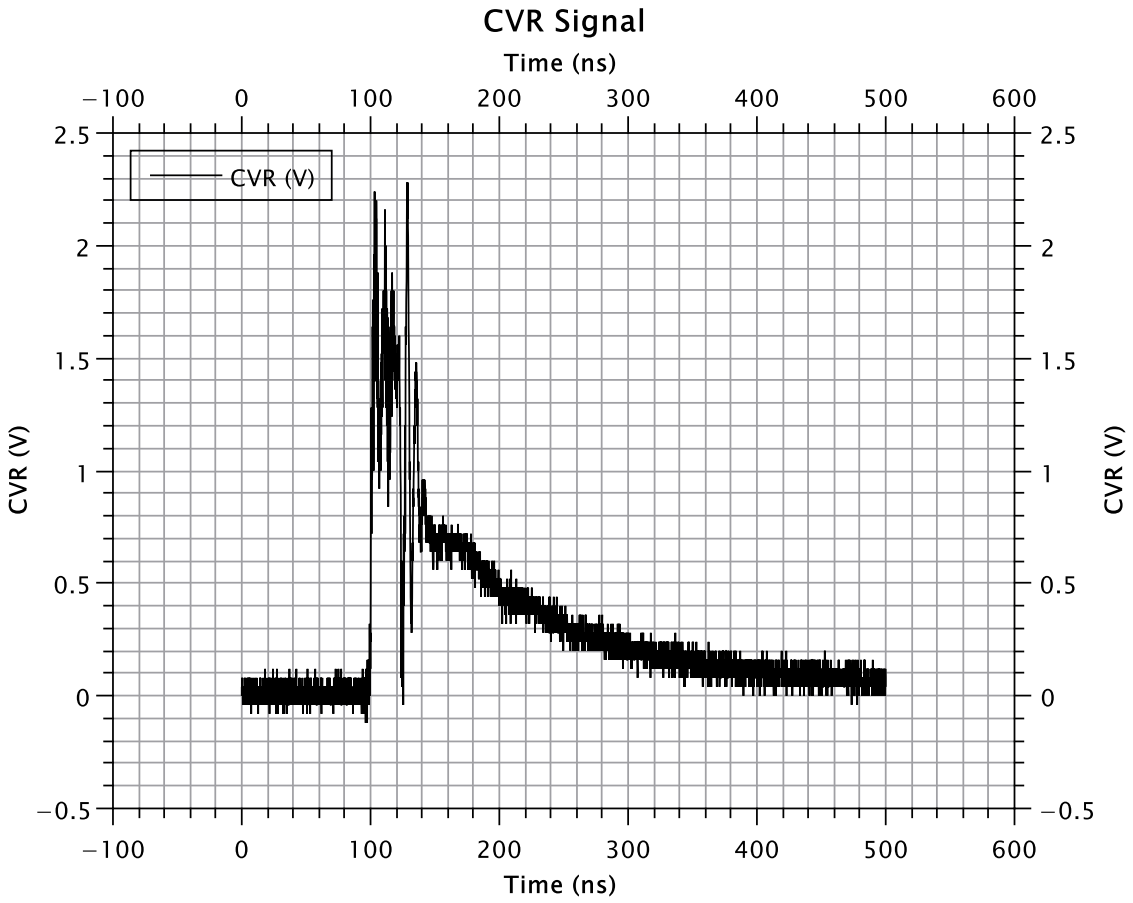

Figure 3-19: CVR signal from a flashover event.

These measurements are gathered by a DPO 7254 2.5 GHz Tektronix oscilloscope [24]. The oscilloscope, laptop controller, and delay generator were put into a shielded data acquisition box, as seen in Figure 3.20, to protect them from the electromagnetic interference produced by the Marx bank.

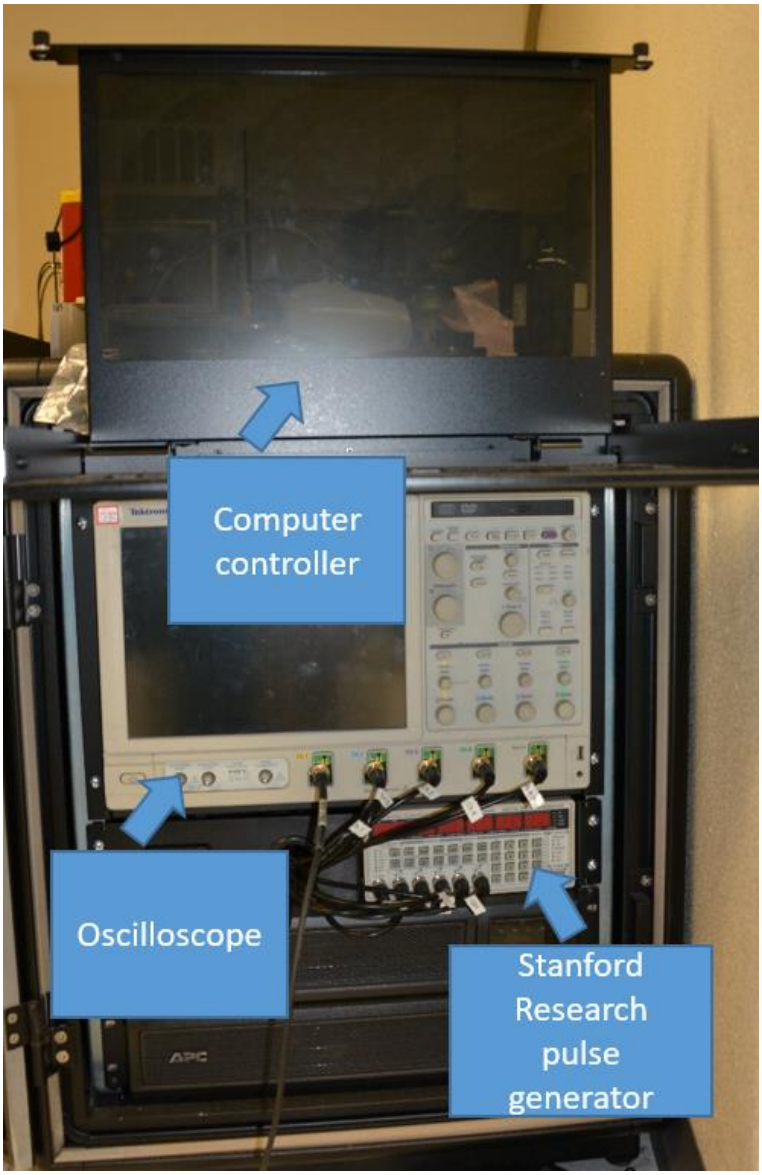

Figure 3-20 The data acquisition box. It is shielded to reduce the EMI effects. The box contains the oscilloscope, the DG, and the computer that controls the experiment.

3.2 Experimental Process

The HGI and monolithic aluminum nitrate samples were sent to UNM in vacuum sealed bags after being baked by the Siena Technologies. The only treatment that UNM performed on the ceramic samples was cleaning them with isopropanol. The samples were handled with gloves, and loaded into the vacuum chamber immediately after cleaning.

To start the vacuum process, the scroll pump is used to reduce the pressure in the chamber to about .05 Torr. At this point the turbo pump can be operated and will take the vacuum chamber pressure to approximately 10^{-7} Torr. This is the pressure minimum of the experimental setup. When the desired vacuum has been achieved the cathode plate is moved to compress the test sample between the anode and the cathode as seen in Figure 3.21.

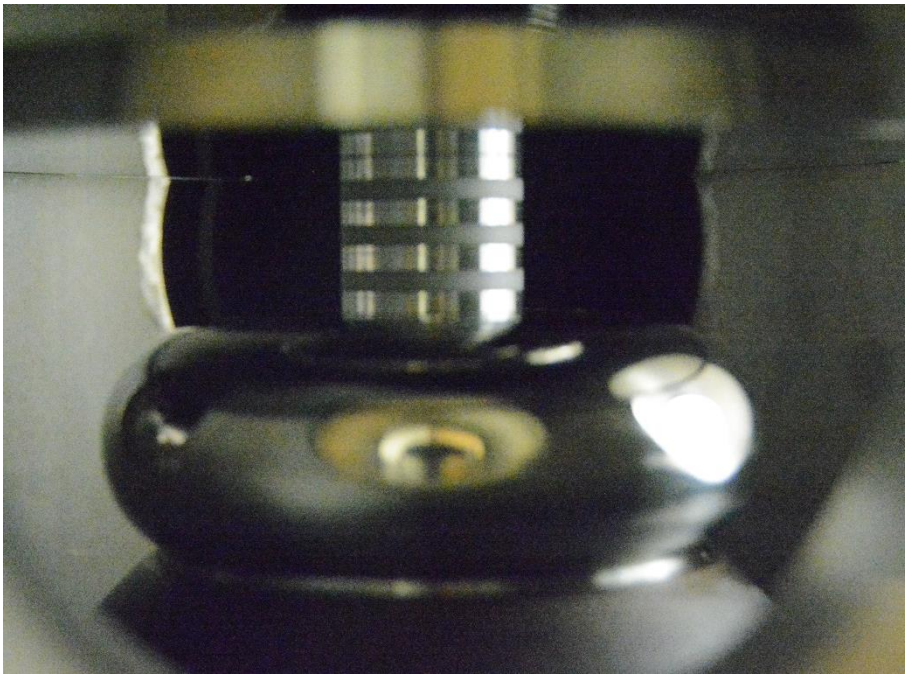

Figure 3-21: A HGI sample loaded into the vacuum chamber lightly compressed between the anode and cathode.

The pressure controller is used to fill the Marx with pressurized nitrogen. Depending on the desired charge voltage the pressure inside the Marx bank will vary. Finally, a Nikon D7100 camera is used to take open shutter pictures if surface flashover occurs. This is not an automated system, but once the user sees evidence for vacuum surface flashover in the waveforms the next shot is recorded using the camera and often vacuum surface flashover is captured as seen in Figure 3.22.

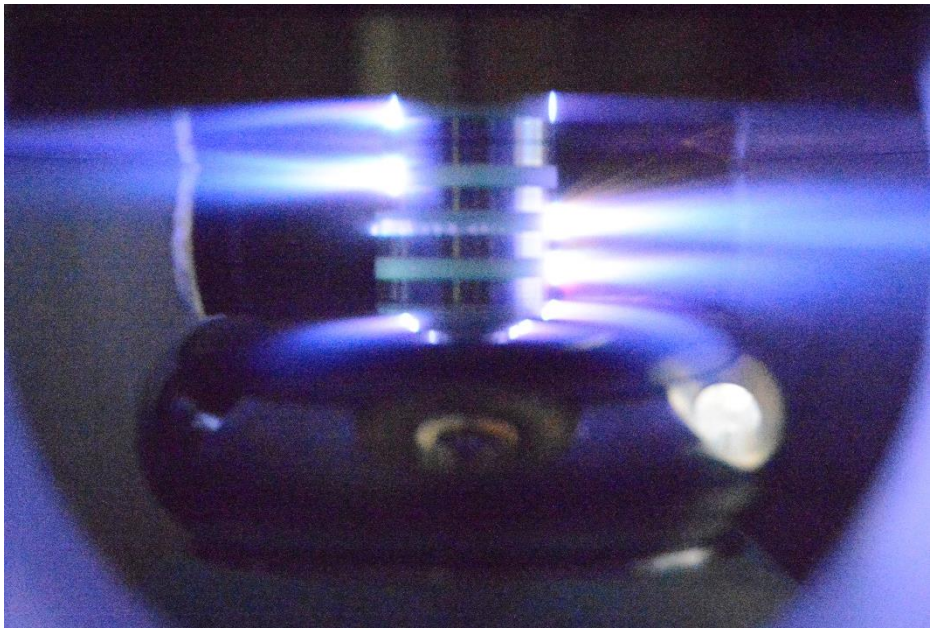

Figure 3-22: An HGI sample experiencing vacuum surface flashover.

Charge voltage of the Marx was increased gradually. If the sample was able to holdoff 5 to 10 pulses the charge voltage would be increased by 1kV. This process was continued until either vacuum surface flashover occurred on the surface of the sample or vacuum surface flashover occurred on the surface of the vacuum feedthrough. Each pulse generated a CVR and D-dot signal and the measurements were kept for analysis. When vacuum surface flashover was seen the electric field holdoff was calculated using the peak voltage and the length of the sample.

Chapter 4

Results

4.1 Comparison of Secondary electron yield

With association with Sienna technologies, UNM decided to focus testing on the ceramic aluminum nitrate (AlN). This ceramic is a vacuum compatible material and can be baked at 400C which was done by Sienna Technologies. Sienna Technologies was able to make different

formulations of AlN using proprietary methods. Each version of AlN had different measured secondary electron yield curves as seen in figure 4.1. According to the literature, material having a lower yield will be able to holdoff more voltage [1]. At operating voltages near 200kV the yield for ST200 is less than that of HY4TN2.

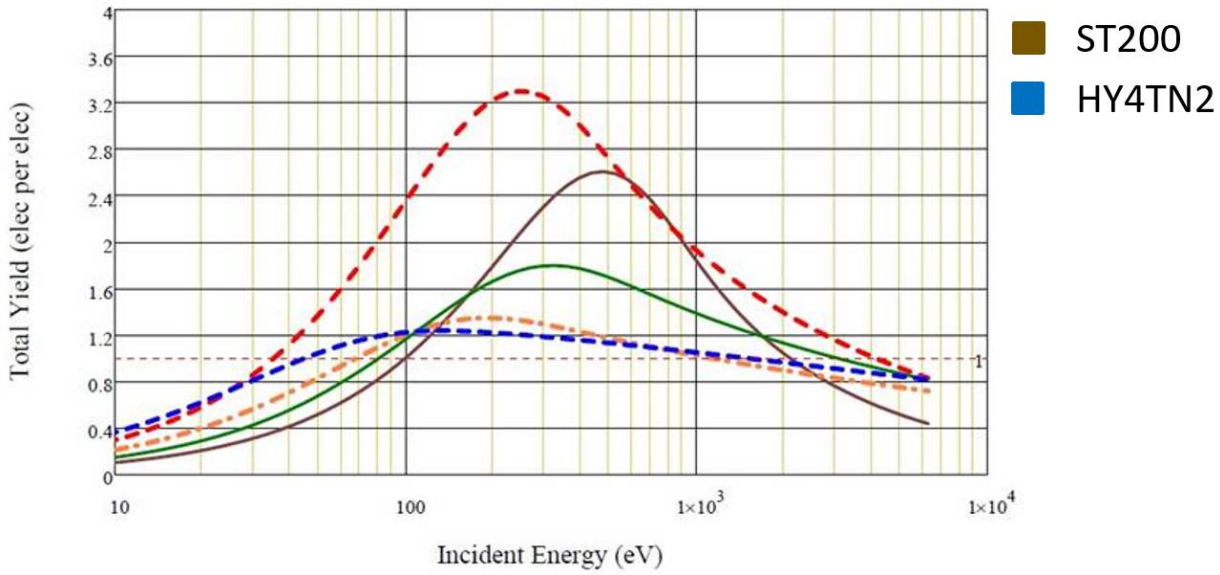

Figure 4-1: The yield curves for different ceramics. ST200 (solid brown), HY4TN2 (dashed blue).

UNM compared two versions of AlN, HY4TN2 and ST200. Insulator samples of each version were made to have the same size and had copper ends attached to reduce the effects of field shaping due to voids being present at the triple points. As expected from the measured electron yield results, the ST200 sample was able to holdoff more voltage after a brief conditioning phase as seen in figure 4.2. The ST200 sample initially performed worse than the HY4TN2 sample, but after conditioning was able to holdoff 150kV. The HY4TN2 sample never experienced conditioning as seen in figure 4.3. Both samples eventually failed due to tracking along the surface.

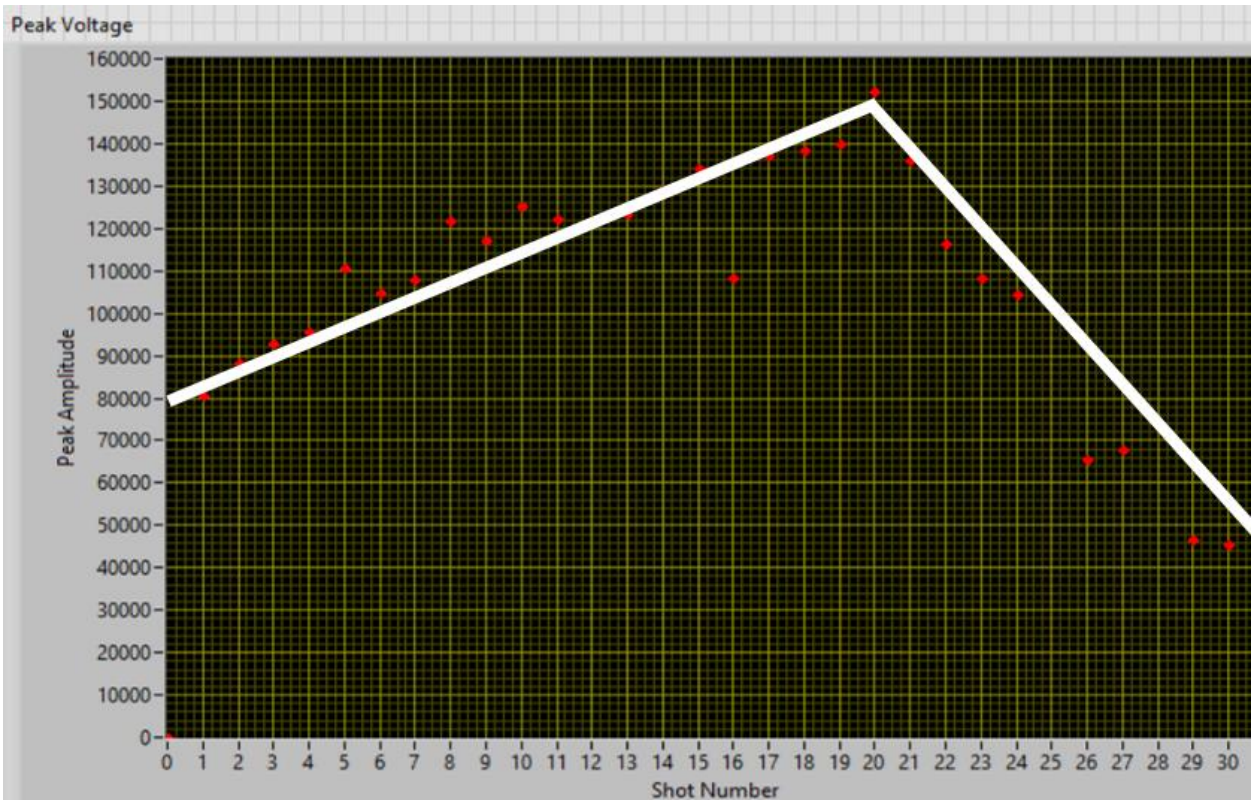

Figure 4-2: Results of ST200 testing.

Figure 4.2 above shows the peak voltage vs the shot number for the ST200 sample. The sample was 1cm in length and able to holdoff more voltage in subsequent shots due to sample conditioning. Each shot on this sample was a 200kV pulse with a 500ns pulse width. Around shot 21 the sample formed a track along the surface. The track made the holdoff voltage fall about 50kV and consistently failed there.

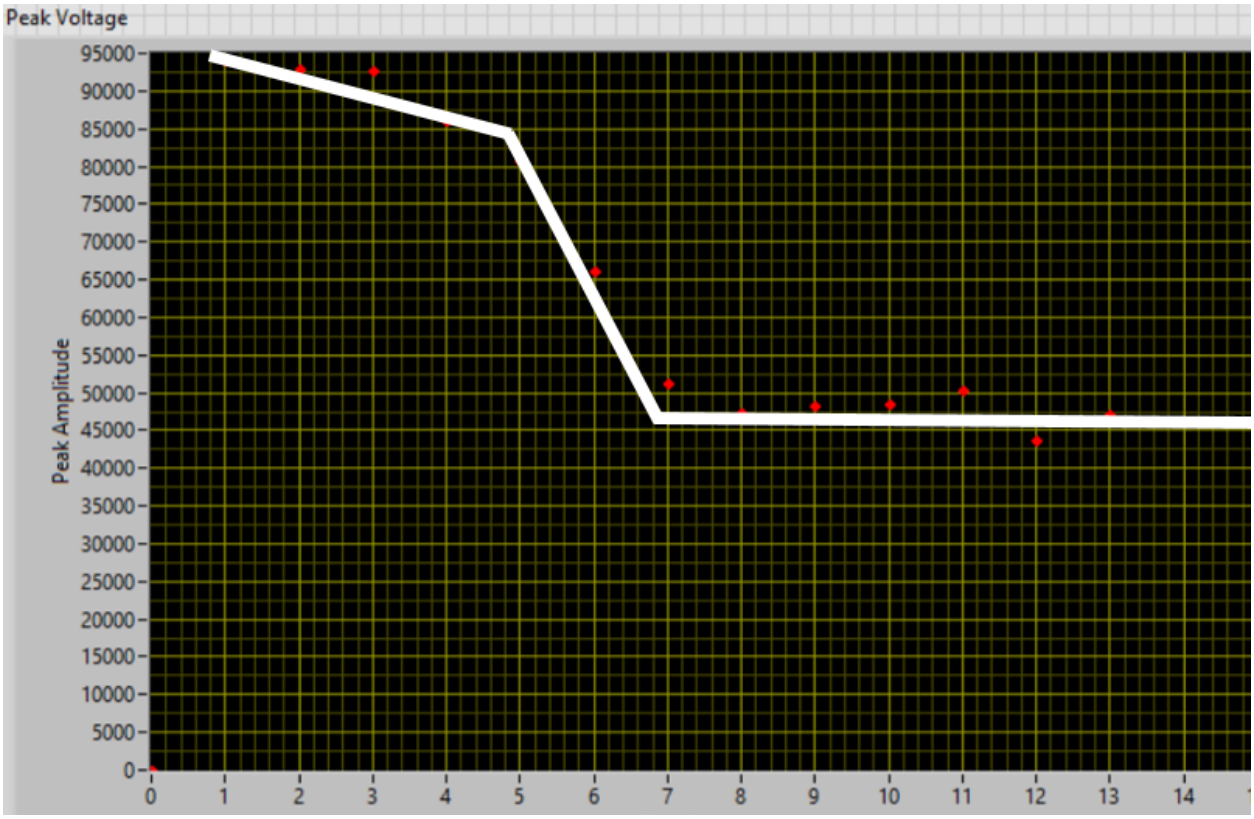

Figure 4-3: Results of HY4TN2 testing.

Figure 4.3 shows the peak voltage vs the shot number for the 1cm long HY4TN2 sample. The sample never experienced any conditioning and the holdoff voltage only got worse. Each shot on this sample was a 200kV pulse with a 500ns pulse width. Around shot 5 the sample formed a track along the surface. The track made the holdoff voltage fall about 50kV and consistently failed there. These results agreed with the literature because the sample with the lower secondary electron yield heldoff more voltage. Due to this behavior, most AlN insulator samples were made out of the ST200 composition, however two of the HGI samples were made out of an AlN composition named Ker due to availability of material.

4.2 Monolithic AlN Insulators

A baseline holdoff voltage for monolithic AlN insulators needed was measured in order to compare to previous results reported for a similar type of insulator. Six total straight wall cylindrical samples were tested and the average electric field holdoff was used for the comparison.

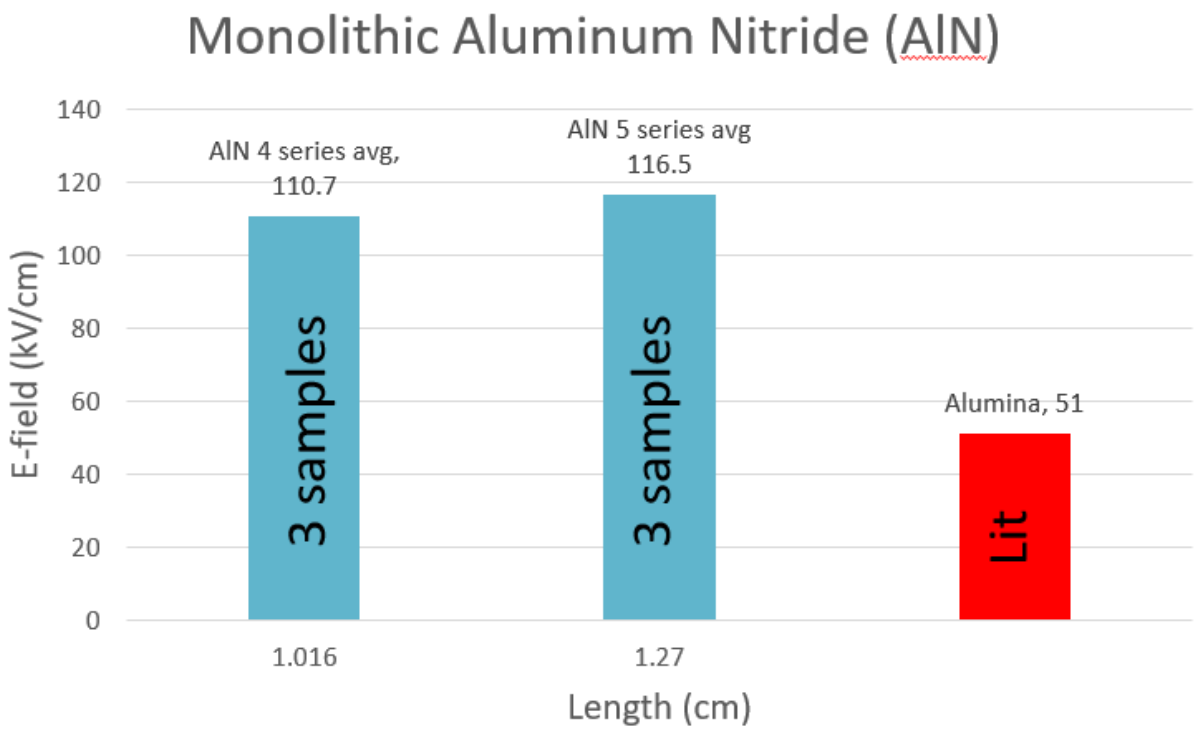

Figure 4-4 Comparison of monolithic AlN and monolithic alumina insulators.

Figure 4.4 compares the average electric field the samples were able to holdoff of two different sizes of monolithic AlN insulators to that of the of an alumina insulator. The alumina samples height was not given, however the assumption is that the sample is between 1.6cm to 2cm because that was the size of the samples Leopold used in his experiments [14]. Figure 4.4 shows that the average AlN insulator had an electric field holdoff over double the alumina insulator.

4.3 Conical Monolithic AlN Insulators

Conical insulators with varying angled slopes have a larger holdoff voltages compared to straight wall insulators due to the behavior of the electric field lines at the triple point [8]. Similar results have been found with the AlN insulator samples. The tested conical AlN samples include two different sizes and two different angles as seen in figure 4.5.

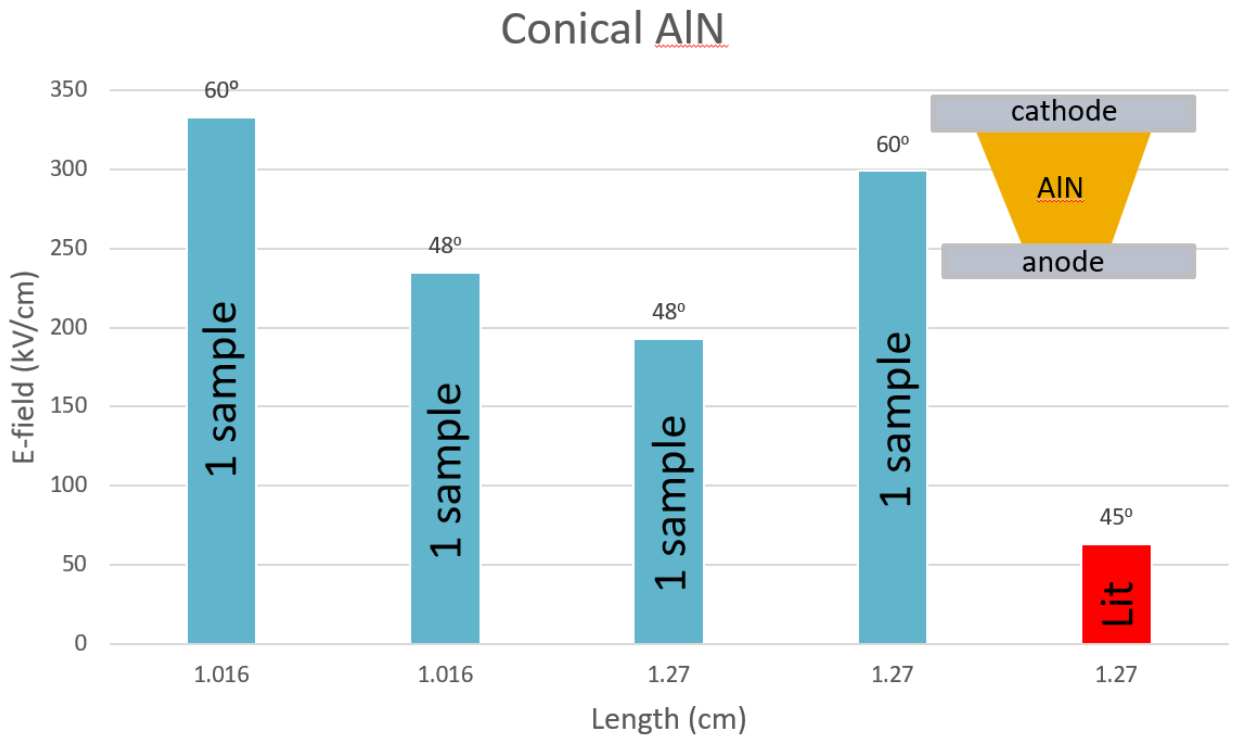

Figure 4-5: The results of the conical AlN testing. Blue bars were tested at UNM. Red bar was taken from the literature [8].

The red bar denotes the measured results of a coated alumina sample found in the literature [8]. AlN insulators are able to holdoff a much larger electric field. However, it should be noted that a 2μs voltage pulse was used in the coated alumina experiment. It is not a direct comparison, however that data implies that the conical AlN may to holdoff more voltage compared to alumina. The results indicate that a 60 degree sample held off the largest electric field, however,

more testing should be done to determine an average holdoff field. These four data points are taken from four different samples. Therefore, there may have been some variation between samples due to surface anomalies or other factors.

4.4 HGI results

The high gradient insulators tested were primarily made from aluminum nitrate (AlN) insulating ceramic and molybdenum (Mo) conductor, however is some cases copper (Cu) was used as the conducting material. Due to ease of manufacturing the thin layered samples were made using copper, however future experimentation should be done using thin layered molybdenum. Leopold et al reported that HGI's will have the largest holdoff field when the insulator to metal ratio (I/M) approached a value of 3 [5] when testing with a fixed cell length. However, the Livermore group reported that an I/M ratio approaching infinity is optimal [7] while using thinner cell lengths. A key differences in the two methods is the amount of layers in the insulator, and the overall size of material per layer. The results indicate that if thin/many layers are used, a larger I/M will have a higher the holdoff. If thick/few layers are used, the highest holdoff approached 3. Our results agree with both authors, however having a thin/many layered sample will holdoff the largest electric field. The following table and graphs are the results.

Sample Id	Sample	Material	height in cm	max voltage (in kV)	E-field in kV/cm	I/M (period)	layer length conductor in cm	layer length insulator in cm
A	HS-728 Refurbished	4Mo/3AlN	1.87	180	96.3	0.67	0.300	0.200
B	HS 729 Refurbished	4Mo/3AlN	2.14	182	85.0	1.00	0.300	0.300
C	HS-730 Refurbished	4Mo/3AlN	1.84	152	82.6	0.67	0.300	0.200
D	HS 755	4Mo/3AlN	1.96	205	102	3.00	0.150	0.450
E	HS 767	4Mo/3AlN	1.98	200	101	2.52	0.170	0.429
F	HS 762	22AlN/21Cu	1.63	105	64.4	2.50	0.020	0.050
G	HS 768-1	22AlN/21Cu	1.19	200	168	10.00	0.005	0.051
H	4 Kovar - 3AlN	4Ko/3AlN	1.53	75	49	0.67	0.255	0.171
I	KER 22 sample 1 AlN	22KER/21Cu	1.59	65	41	12.50	0.005	0.064
J	KER 22 sample 2 AlN	22KER/21Cu	1.58	160	101	12.50	0.005	0.064
K	HS-728 AlN	4Mo/3AlN	1.87	140	75	0.67	0.300	0.200
L	HS-729 AlN	4Mo/3AlN	2.14	220	103	1.00	0.300	0.300
M	HS-730 AlN	4Mo/3AlN	1.84	180	98	0.67	0.300	0.200
N	7 layer AlN	7Cu/6AlN	1.5	97.5	65	41.50	0.006	0.243
O	HS 772-2	4Mo/3AlN	1.93	180	93.3	2.00	0.191	0.381
P	HS 772-1	4Mo/3AlN	2.11	96	45.5	1.00	0.300	0.300

Table 1: The details of the samples tested. Each sample has been given a corresponding letter so that the sample can be easily identified in the following charts.

Table 1 gives the holdoff field of the sample, total length of the sample, and lengths of each layer in each sample. Sample HS 768-1 (Sample G) had the largest holdoff field. This sample is a Livermore style HGI constructed of 22 thin layers of AlN and 21 thin layers of Cu. This HGI is one of the shortest samples tested at 1.19 cm tall. The I/M ratio of this sample is 10. Sampayan suggested that insulator's electric field holdoff follow a $\frac{1}{\sqrt{L}}$ distribution [8]. If this is the case the results should indicate that the HGI with the thinnest insulating layer will have the largest electric field. The following graphs will be a comparison of the electric field vs the metal layer length, the insulator layer length, the total length of the sample, and the I/M ratio.

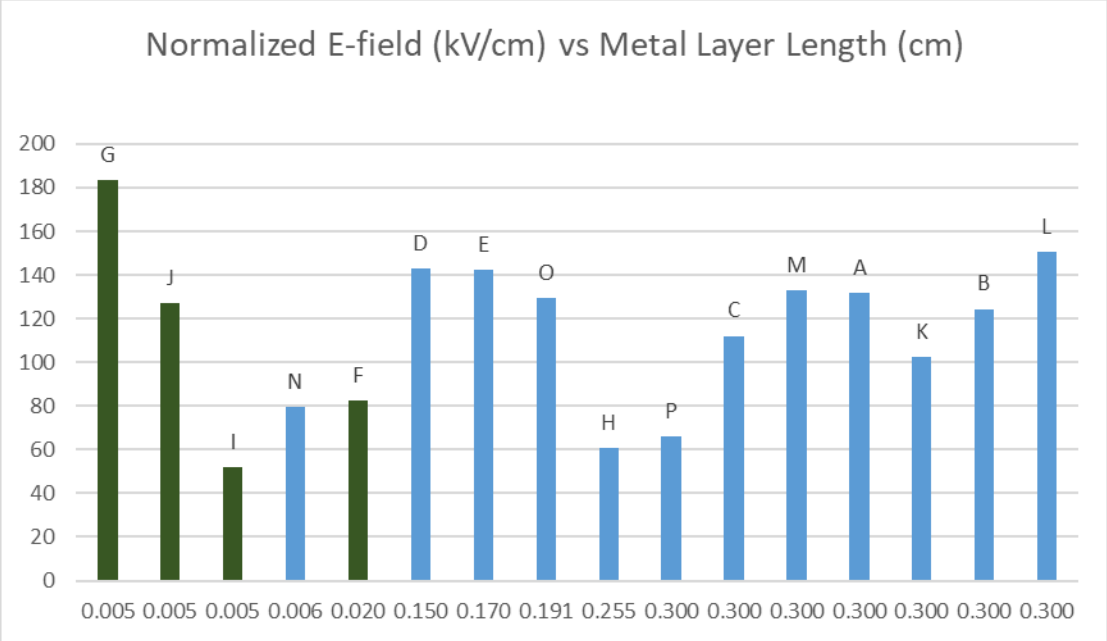

Figure 4-6: This graph shows the holdoff electric field vs the length of the metal layers that make up the HGI sample. The largest holdoff field came from the sample with the smallest metal layer

length. The green bars represent HGI samples with thin layers. The blue bars represent thick layers.

Leopold et al suggested that a conducting layer needs to be thicker in order to modify the electric field next to the surface enough to push electrons away from the surface [5]. To verify that this dependence is associated with the I/M ratio and not the length of a metal layer figure 4.6 was made. This graph shows that the thinnest metal layer heldoff the largest electric field and as the metal layer got larger no trend in decline in performance can be seen.

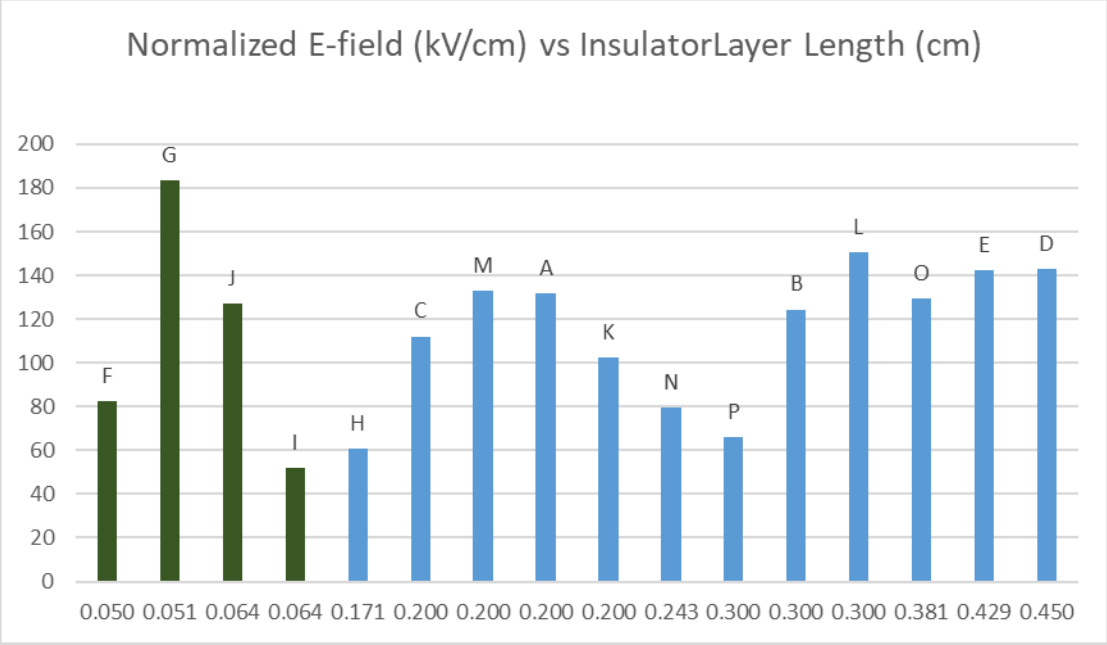

Figure 4-7: This graph shows the holdoff electric field vs the length of insulating layers. The largest heldoff field came from the 2nd smallest length of insulator. The green bars represent HGI samples with thin layers. The blue bars represent thick layers.

The $\frac{1}{\sqrt{L}}$dependence suggests that the smaller the insulator the lager the holdoff electric field. If HGIs are many insulators stacked on top of each other and the $\frac{1}{\sqrt{L}}$is applicable, the largest field should be expected to also have the smallest insulator layer length. Figure 4.7 shows that

the smallest insulator did not holdoff the largest electric field, however the second smallest insulator sample did. Looking at the remaining data, no trend is clear. The $\frac{1}{\sqrt{L}}$ dependence should not be ruled out. HGI samples can be difficult to make, it is possible that sample F had surface anomalies that encouraged vacuum surface flashover. Also samples L,O,E, and D all performed about as well as sample J, this is a problem for the $\frac{1}{\sqrt{L}}$ trend.

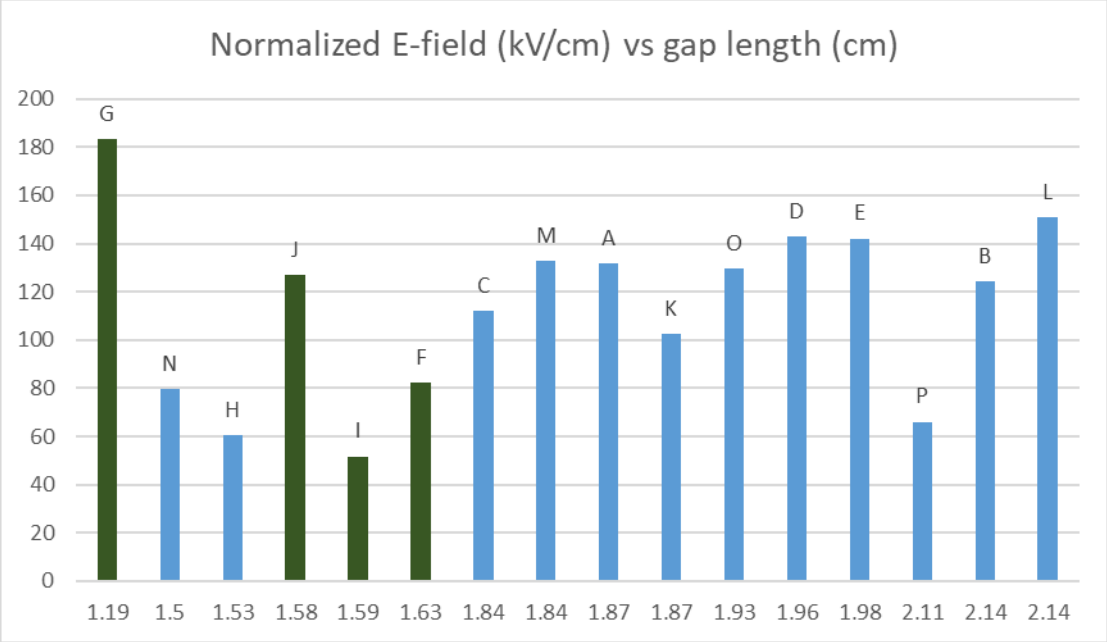

Figure 4-8: This graph shows the holdoff electric field vs the total length of the HGI. The largest holdoff field came from the smallest sample. Sample L heldoff an electric field of 103 kV/cm. This is the second largest holdoff. The green bars represent HGI samples with thin layers. The blue bars represent thick layers.

Figure 4.8 evaluates the holdoff electric field versus the total length of the HGI. Sample G was the smallest insulator and had the largest holdoff field. Sample L was the largest sample and had the second largest holdoff electric field. It should be noted that most thick/few layered HGIs heldoff an electric field around 100 kV/cm.

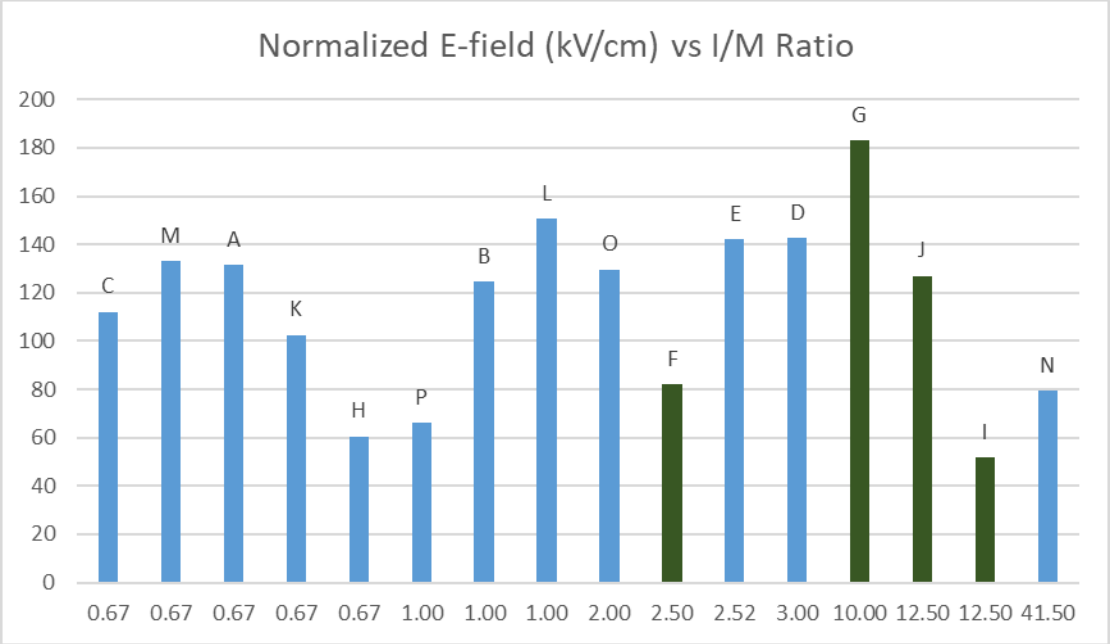

Figure 4-9: This graph shows the holdoff electric field for each I/M ratio. It can be seen that as the ratio approaches 3 there is an increase in performance. However, samples M and L perform about as well as samples D and E. Sample G has an I/M ratio of 10 and was the only sample with an I/M > 3 to holdoff a much larger electric field. The green bars represent HGI samples with thin layers. The blue bars represent thick layers.

Livermore proposed that HGI samples will continue to improve as the I/M ratio approached infinity (some point before the sample is monolithic) [7]. Livermore used samples that had thin conducting and insulating layers. Sample G is a Livermore style insulator and had the largest holdoff electric field as seen in figure 4.9. Sample F is a Livermore style many thin layered model, however the I/M ratio approaches 3 and the sample did not perform well. Leopold used thick conducting and insulating layers and proposed that the optimal I/M ratio approaches 3 [5]. Sample D is a Leopold style HGI and was able to holdoff 101kV/cm. This result agrees with the results that Leopold gathered. Sample N is made of thick insulating layers and thin conducting layers resulting in an I/M ratio of 41.5. This sample did not perform well. It

is difficult to draw conclusions on the thin HGIs. More data should be taken, however it should be noted that sample G had the largest electric field holdoff by about 60kv/cm.

Chapter 5

Discussion

5.1 Summary

Surface flashover in vacuum is typically the limiting factor in high voltage experiments. Using different insulator materials or geometries have shown to increase the holdoff voltage [1]. The results seen in chapter 4 show that the largest electric field holdoff was achieved by a conical AlN sample with a 60° slope. This sample was able to holdoff an electric field of $333\frac{kV}{cm}$. Depending on application, conical samples are not always ideal and high gradient insulators should be considered. A high gradient insulator was able to holdoff an electric field of $168\frac{kV}{cm}$. This is an increase of $50\frac{kV}{cm}$ compared to monolithic AlN insulators of similar size.

Two approaches of high gradient insulator were explored in this work. The first approach (Leopold) used a few thick layers of insulating and conducting material and the second approach (Livermore) used many thin layers of the materials. Each approach suggested a different I/M ratio and had experimental results to support their claims [5] [7]. This work showed that both approaches of HGIs worked, however we observed the Livermore approach was able to holdoff the largest electric field, although this conclusion depends on a single high-performing sample.

5.2 Future Work

This work showed that a thin layered sample was able to holdoff the largest electric field, although the superior performance of sample G ought to be reproduced. The effects of the I/M ratio remain unclear. Data on thick versus thin metal layers samples having identical insulating

layer length may provide a more definitive dataset. Additionally, if total lengths were kept constant this data might provide more insight into the effects of the conducting layers. Monolithic insulators made of 3D printed resin material will also be tested. The 3D printer can make the lengths of the insulators precise and the $\frac{1}{\sqrt{L}}$ dependence can be tested in this way.

References

[1] H. C. Miller, "Surface Flashover of Insulators," *IEEE Transactions on Electrical Insulation,* vol. 24, no. 5, pp. 765- 786, 1989.

[2] R. A. a. J. Brainard, "Mechanism of Pulsed Surface Flashover Involving Electron-Stimulated Desorption," *Journal of Applied Physics,* vol. 51, pp. 1414-1421, 1980.

[3] N. M. Jordan, "Electric field and electron orbits near a triple point," *Journal of Applied Physics,* no. 102, 2007.

[4] V. Sampayan, "Multilayer Ultra-High Gradient Insulator Technology," *Int. Symp. on Discharges and Electrical Insulation in Vacuum-Eindhoven,* pp. 740-743, 1998.

[5] J. Leopold, "Different Approach to Pulsed High-Voltage Vacuum-Insulation Design," *Physical Review of Special Topics- Accelerators and Beams,* vol. 10, 2007.

[6] J. G. Leopold, "Optimizing the Performance of Flat-surface, High-gradient Vacuum Insulators," *IEEE Transactions on Dielectrics and Electrical Insulation,* vol. 12, no. 3, pp. 530-536, 2005.

[7] J. R. Harris, "Vacuum Insulator Development for the Dielectric Wall Accelerator," *Journal of Applied Physics* , vol. 104, no. 023301, pp. 023301-1 - 023301-8, 2008.

[8] O. Milton, "Pulsed Flashover of Insulators in Vacuum," *IEEE Transactions on Electrical Insulation,* vol. 7, no. 1, pp. 9-15, 1972.

[9] A. S. P. a. R. Hackam, "Influence of Metal-Insulator Junction on Surface Flashover in Vacuum," *Journal of Applied Physics,* vol. 61, no. 11, pp. 4992-4999, 1987.

[10] P. Yan, "Experimental Investigation of Surface Flashover in Vacuum using Nanosecond Pulses," *IEEE Transactions on Dielectrics and Electrical Insulation,* vol. 14, no. 3, pp. 634-642, 2007.

[11] G. F. Dionne, "Origin of secondary-electron-emission yield-curve parameters," *Journal of Applied Physics,* vol. 46, no. 8, pp. 3347-3351, 1975.

[12] R. S. a. B. Williams, "Secondary-Electron Emission," *IEEE Transactions on Nuclear Science,* vol. 15, no. 3, pp. 167-170, 1968.

[13] M. Pivi, "Sharp reduction of the secondary electron emission yield from grooved surfaces," *Journal of Applied Physics,* vol. 104, 2008.

[14] A. Neuber, "The role of outgassing in surface flashover under vacuum," *IEEE Transactions on Plasma Science* , vol. 28, no. 5, pp. 1593-1598, 2000.

[15] E. W. Gray, "Vacuum surface flashover: A high-pressure phenomenon," *Journal of Applied Physics,* vol. 58, no. 1, 1985.

[16] H. M.-G. a. M. S. W. Gorczewski, "Development of an Insulator for 50 Hz, 110 kV Operation in Vacuum," *Int. Symp. on Discharges and Electrical Insulation in Vacuum-Eindhoven,* pp. 399-404, 1972.

[17] J. Harris, "Electrical strength of mulilayer vacuum insulators," *Applied Physics Letters,* vol. 93, no. 24, 2008.

[18] "T&M Research Products, Inc.," 2015. [Online]. Available: https://www.tandmresearch.com/index.php?mact=ListIt2Products,cntnt01,detail,0&cntnt01item=series-sdn-414&cntnt01template_summary=Side&cntnt01returnid=19. [Accessed 27 January 2020].

[19] "Agilent Products- Vacuum Technologies," Agilent, 2020. [Online]. Available: https://www.agilent.com/en/products/vacuum-technologies. [Accessed 27 January 2020].

[20] "National Instruments Products - Labview," National Instruments, 2020. [Online]. Available: https://www.ni.com/en-us/shop/labview.html. [Accessed 27 January 2020].

[21] Ensinger, "San Diego Plastics, Inc. - Ultem," San Diego Plastics, [Online]. Available: http://www.sdplastics.com/ensinger/ultem.pdf. [Accessed 27 January 2020].

[22] Dassault Systems, "3ds-products-services-CST studio suite," Dassault Systems, 2020.] [Online]. Available: https://www.3ds.com/products-services/simulia/products/cst-studio-suite/. [Accessed 27 January 2020].

[23] North Star High Voltage, "North Star High Voltage- probes," Noth Star High Voltage, 2014. [Online]. Available: http://www.highvoltageprobes.com/high-voltage-probes. [Accessed 27 January 2020].

[24] Tektronix, "Tektronix-Oscilloscopes," Tektronix, 2020. [Online]. Available: https://www.tek.com/oscilloscope. [Accessed 27 January 2020].